Missouri S&T Library and Learning Resources

Scholars' Mine

Masters Theses

Student Theses and Dissertations

Summer 2011

Analysis and modeling of depth-of-cut during end milling of deposited material

Haythem Gaja

Follow this and additional works at: https://scholarsmine.mst.edu/masters_theses

 Part of the Manufacturing Commons

Department:

Recommended Citation

Gaja, Haythem, "Analysis and modeling of depth-of-cut during end milling of deposited material" (2011). *Masters Theses*. 4988.
https://scholarsmine.mst.edu/masters_theses/4988

This thesis is brought to you by Scholars' Mine, a service of the Missouri S&T Library and Learning Resources. This work is protected by U. S. Copyright Law. Unauthorized use including reproduction for redistribution requires the permission of the copyright holder. For more information, please contact scholarsmine@mst.edu.

ANALYSIS AND MODELING OF DEPTH-OF-CUT DURING END MILLING OF DEPOSITED MATERIAL

by

HAYTHEM GAJA

A THESIS

Presented to the Faculty of the Graduate School of the

MISSOURI UNIVERSITY OF SCIENCE AND TECHNOLOGY

In Partial Fulfillment of the Requirements for the Degree

MASTER OF SCIENCE IN MANUFACTURING ENGINEERING

2011

Approved by

F. W. Frank Liou, Advisor
Robert G. Landers
Joseph W. Newkirk

© 2011
Haythem Gaja
All Rights Reserved

ABSTRACT

This study addresses depth-of-cut detection and tool-workpiece engagement using an acoustic emission monitoring system during milling machining for a deposited material. Online detection of depth-of-cut presents many technical difficulties. Researchers have used various types of sensors and methods to assess the depth-of-cut and surface errors. Due to the strong correlation between acoustic emission and cutting depth during the depth end milling process, it is useful to forecast the depth-of-cut from the acoustic emission signal. This work used regression analysis to model and detect the depth-of-cut. The experiments were carried out on a Fadal vertical 5-Axis computer numerical control machine using a carbide end-mill tool, and a piezoelectric sensor (Kistler 8152B211) was used to acquire the acoustic emission signal. A National Instruments real-time system, combined with a National Instruments LabVIEW graphical development environment, was used as a data acquisition system. A series of experiments were conducted to create a depth-of-cut model. The inputs were used to predict depth-of-cut are the identified root mean square of the acoustic emission, spindle speed, feed rate, and tool status. The effects of these inputs were evaluated using a fractional factorial design-of-experiment approach.

ACKNOWLEDGMENTS

I would like to express my sincere gratitude to my advisor Dr. Frank Liou for his support, patience and invaluable help throughout my master's research and study.

I would like to thank Dr. Newkirk and Dr. Landers for their sound advice and guidance during my research and study. I deeply appreciate them for being my thesis committee members.

I would also like to thank all the members in the LAMP lab, especially Todd Sparks for making my research and study at MST valuable and memorable.

Last but not least, I would like to give my special thanks to my family back home in Libya for their love and support which enabled me to complete this work.

TABLE OF CONTENTS

Page

ABSTRACT……...……. iii

ACKNOWLEDGMENTS……...……... iv

LIST OF ILLUSTRATIONS……..... vii

LIST OF TABLES……..... ix

NOMENCLATURE…… x

1. INTRODUCTION……..... 1

1.1 THE NEED FOR A DEPTH-OF-CUT DETECTION SYSTEM……..... 1

1.2 RESEARCH OBJECTIVES……..... 2

2. BACKGROUND AND LITERATURE REVIEW……..... 3

2.1 MONITORING OF MACHINING OPERATIONS……..... 3

2.2 ACOUSTIC EMISSIONS……. 3

2.3 THE ACOUSTIC EMISSION SENSOR……..... 5

2.4 ACOUSTIC EMISSION SIGNAL SOURCES…… 6

2.5 FEATURES OF THE ACOUSTIC EMISSION SIGNAL……... 9

2.6 ROOT MEAN SQUARE SIGNAL ANALYSIS……..... 10

2.7 ACOUSTIC EMISSION SIGNAL PROCESSING……..... 12

2.8 DEPTH-OF-CUT DETECTION……... 13

3. RESEARCH METHODOLOGY……... 15

3.1 INTRODUCTION…… 15

3.2 ACOUSTIC EMISSION SYSTEM……..... 16

3.3 EXPERIMENTAL SETUP……... 20

3.4 TOOL STATUS CATEGORIZATION…… 21

4. ANALYSIS AND MODELING……..... 26

4.1 THE RAW ACOUSTIC EMISSION SIGNAL…… 26

4.2 MOVING AVERAGE AND SPIKES REMOVAL……. 28

4.3 THE ACOUSTIC EMISSION SIGNAL SENSITIVITY TO DEPTH-OF-CUT CHANGES……..…... 33

4.4 DESIGN OF EXPERIMENTS……..... 33

5. RESULTS AND DISCUSSION……..... 39

5.1 STATISTICAL RESULTS OF EXPERIMENTAL DATA……..... 39

5.2 THE ESTIMATED RMS^2..... 42

5.3 ESTIMATION OF DEPTH-OF-CUT……..... 43

6. CONCLUSIONS AND RECOMMENDATIONS FOR FUTURE WORK..... 51

6.1 CONCLUSIONS……...…… 51

6.2 FUTURE WORK…….....… 51

BIBLIOGRAPHY……...… 53

VITA…….. 55

LIST OF ILLUSTRATIONS

Figure Page

2.1. Steps of the Depth-of-Cut Monitoring Process……..……..... 4

2.2. Assembly of an Acoustic Emission Sensor……...…….. 7

2.3. Acoustic Emission Sources During Metal Cutting and Arrows Indicate the Acoustic Emissions…… 8

2.4. Types of Acoustic Emission in the Metal-cutting Process……...…..…… 9

2.5. Acoustic Emission Signal Feature…….…..... 11

3.1. Kistler 8152B111 Acoustic Emission Sensor……...…... 17

3.2. Piezotron Coupler…… 18

3.3. The Coupler Assembly Diagram……..... 19

3.4. Experimental Setup……...……... 20

3.5. Tool Wear for 0.5 Inch End Mill……..…... 22

3.6. Fresh Tool (The Wear = 10 μm)……..... 23

3.7. Worn-out Tool (The Wear = 320μm)……..... 24

3.8. Typical Taylor Tool Wear Curve……..……... 25

4.1. The Raw Signal (2 mm depth-of-cut, 5500 RPM spindle speed and 100 mm/min feed rate)……..……..……... 27

4.2. Root Mean Square at the Engagement Region…….……... 29

4.3 Axial Slot Milling……..……... 30

4.4. Root Mean Square at Disengagement Region……..…... 31

4.5 (a) The Original Acoustic Emission Signal (b) The Signal after Removing the Spikes…….…… 32

4.6 The Acoustic Emission Sensitivity to the Depth-of-cut Changes……..…… 34

4.7. Workpiece Geometry……... 38

5.1. Residual Plot for the RMS^2……...……... 39

5.2. Order Plot of the Residuals……...……... 40

5.3. Normal Probability Plot of the Residuals……...……. 41

5.4. The Estimated RMS^2 vs. Actual Values……...…... 42

5.5. Depth-of-cut Estimation…….. 44

5.6. Interrupted Cutting (a) Nominal/Estimated Depth-of-cut (b) Cutting Geometry……..…… 45

5.7 Inclined Surface Cutting (a) Nominal/Estimated Depth-of-cut (b) Cutting Geometry……..…… 46

5.8. Scanned Deposited Material (a) Machined (b) Original (c) Removed…….…... 47

5.9. Machined Material Slicing (a) First Section. (b) Fifteenth Section……..…... 48

5.10. Measured and Detected Depth-of-cut for a Deposited Material…….……... 49

LIST OF TABLES

Table Page

4.1 Factors and Levels Defined for Experimentation…….. 36

4.2. Taguchi L9 (34) Experimental Design …..…….…….. 36

5.1. The Area and Depth-of-cut of the Section …...…...……. 49

NOMENCLATURE

Symbol	Description
T	The Generated Electric Field
C	Sensor Material's Piezoelectric Stress Constant
E	Sensor's Young's Modulus
L	Material Length
ΔL	The Change in Length
V	Voltage Across the Sensor
RMS	Root Mean Square
V (t)	The Signal Function
ΔT	Time Period
T	Engagement or Disengagement Time
D	Tool Diameter
F	Feed Rate
α	Rake Angle
∅	Shear Angle
τ_k	Shear Strength
a_p	Axial Depth-of-cut
U	Cutting Velocity
l	Chip-tool Contact Length
l_l	Length of Sticking Zone
t_l	Feed Load

W	Average Flank Wear Land
N	Cutting Speed

1. INTRODUCTION

1.1 THE NEED FOR A DEPTH-OF-CUT DETECTION SYSTEM

Automation of manufacturing processes has become popular because it increases the quality and accuracy of the parts produced and reduces both costs and production time. However, automated manufacturing of metallic structures has thus far been limited to determination of the building sequence, optimization and evaluation of the feasibility of direction of the machining process.

One of the difficulties using an adaptive control and tool monitoring system is accurate representation of the variation in machining variables such as cutting speed, feed rate, and depth-of-cut. In the end-milling process, particular changes in depth-of-cut must be carefully considered to ensure the effectiveness of the control system.

Previous studies on end-milling has treated depth-of-cut as a constant for simplicity, however, this approach is a distortion of reality. Depth-of-cut is difficult to control because of the irregular shape of workpieces, the imprecision of locating workpieces on the machine, and machining errors from prior cutting. Even if such elements are accurately accounted for before the final machining, the location of the cutter must consistently follow the change in workpiece shape, especially when a complex part is machined. Any effective automation method must address these issues.

One manufacturing process that depends on depth-of-cut detection and monitoring is hybrid manufacturing. The approach of hybrid manufacturing addressed in this study uses two manufacturing processes, one process builds a metal part using laser deposition and the other process finishes the part using a milling process. The ability to produce complete functioning parts in a short time with minimal cost and energy

consumption has made hybrid manufacturing popular in many industries for parts repair and rapid prototyping. Using an acoustic emission signal, the axial depth-of-cut can define a range of calculations for tool deflection and thus for depth-of-cut. This research focuses on detection of the depth-of-cut online during the milling process. Due to deposition defects and uncertainties involved in depositing the required amount of material [2], production of precision surfaces can be challenging. Therefore, a sensing system is necessary to detect the depth-of-cut and tool-workpiece engagement by using an acoustic emission monitoring system.

1.2 RESEARCH OBJECTIVES

This research had two primary objectives. First, it established a methodology to detect an acoustic emission signal, so that the acoustic emission characteristics of the milling could be analyzed. Second, it sought to relate these acoustic data to machining parameters to detect depth-of-cut.

2. BACKGROUND AND LITERATURE REVIEW

2.1. MONITORING OF MACHINING OPERATIONS

Various factors can indicate a change in cutting conditions such as depth-of-cut and tool status. These include force, temperature, and acoustic emissions. In monitoring the machining operations, a range of sensors has been used to evaluate these indicators, and a close correlation has been identified between sensor outputs and specific indicators [1-3, 6, 8-16]. Raw signals must be processed to extract information such as root mean square, amplitude, event, and rise time. Machine operators or a machine tool numerical controller can then use this information to suggest or execute appropriate adaptive or corrective actions [16]. Figure 2.1 illustrates the steps in the depth-of-cut monitoring process. The steps can be surmised as follows:

1- Acquire the acoustic emission signal using a piezoelectric sensor.
2- Extract features, and calculate the root mean square.
3- Process the signal to determine the relationship between the depth-of-cut and the root mean square.
4- Estimate the depth-of-cut using a regression model.
5- Compare the detected depth-of-cut to the required depth-of-cut, and take the appropriate action based on the results.

2.2. ACOUSTIC EMISSIONS

According to the American Society for Testing Materials acoustic emissions are elastic waves emitted from sources inside a material as a result of the sudden release of

energy during metal deformation [22]. Acoustic emissions have been used in many areas, such as tool wear detection and nondestructive testing.

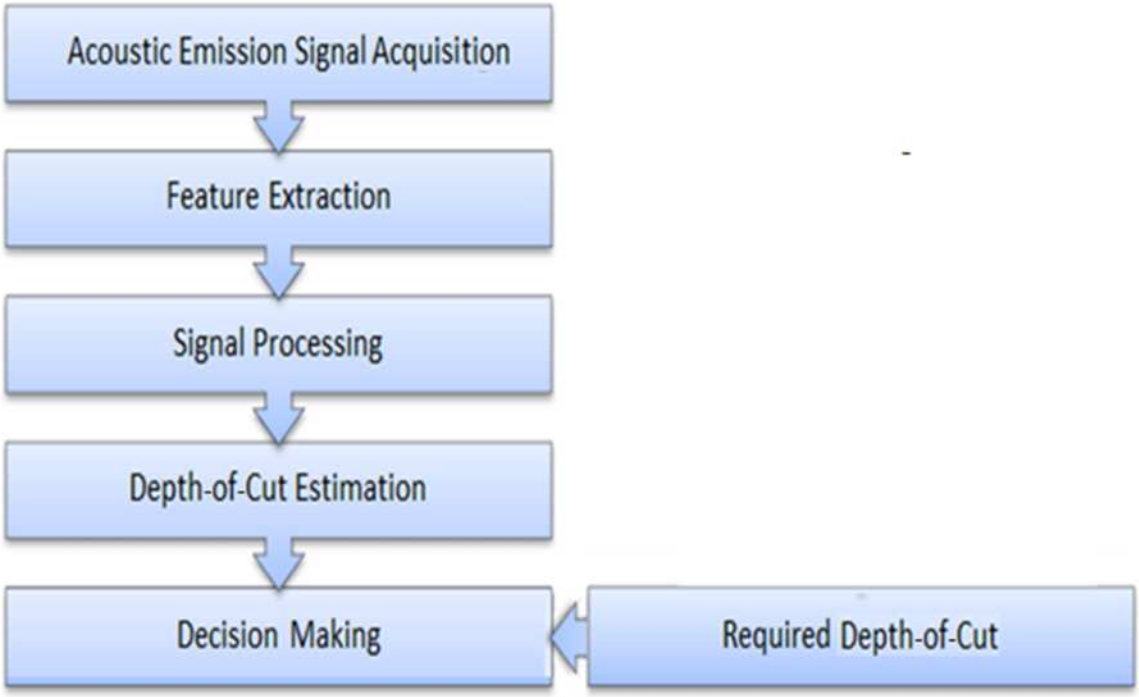


Figure 2.1. Steps of the Depth-of-Cut Monitoring Process

Since Joseph Kaiser's early work in the 1950s many researchers have used the acoustic emission phenomena in non-distractive testing and tool monitoring. Acoustic

emissions have become an important tool for instrumentation and monitoring due to the great advances in signal classification, instrumentation, and sensors. Kaiser was the first to use electronic instrumentation to detect audible sounds produced by metals during deformation [7]. He observed that acoustic emission activity was irreversible. In other words, acoustic emissions do not generate during the reloading of a material until the stress level exceeded the previous high load. This irreversibility has become known as "Kaiser's Effect," and it has proved to be very useful in acoustic emission studies. Kaiser also proposed a distinction between burst and continuous emission, where the acoustic emissions are attributed to friction between grains.

In recent years, acoustic emission sensors designed for the automated manufacturing environment have been very successful. Acoustic emissions occur over a wide frequency range, but most often from 100 kHz to 1 MHz. The main benefit of using acoustic emission sensors in monitoring manufacturing processes is that the vibrations of the machine and ambient noises have a much narrower frequency range than does the acoustic emission signal. Thus, the received signal is mostly free of noise unrelated to the cutting process. However, interpretation of the acoustic emission data requires considerable testing experience and background knowledge.

2.3. THE ACOUSTIC EMISSION SENSOR

The acoustic emission sensor is a piezoelectric transducer usually made from a lead zirconate titanate (PZT), or single crystal materials. These materials generate an electrical charge as a result of applied mechanical force and generate a mechanical force as a result of an applied electrical field. This phenomenon is known as the piezoelectric

effect. The deformation of material produces elastic stress waves which apply mechanical forces on the face of the sensor with very small amplitude. These waves can be detected by the sensor in a wide frequency range but typically from 100 kHz to 1 MHz and convert them into a voltage. Figure 2.2 illustrates the assembly of a piezoelectric sensor. The acoustic emission wave received by the sensor causes stress expressed as E (ΔL/L) where E is the sensor's Young's modulus, L its length, and ΔL is the change in its length [18]. The stress generates an electric field expressed as

$$T = C \times E \left(\frac{\Delta L}{L}\right) \qquad (1)$$

where C is the sensor material's piezoelectric stress constant. The voltage across the sensor, is then

$$V = C \times E \times \Delta L \qquad (2)$$

the usual values of C and E for PZT are 24.4 x 10-3 V rn/N and 58.5 GPa, respectively. With an amplifier a voltage as small as 0.01 mV can be detected.

2.4. ACOUSTIC EMISSION SIGNAL SOURCES

During machining, the load on the material can reach the material's yield stress and the machined material's acoustic emissions are most obvious. At this point, structural

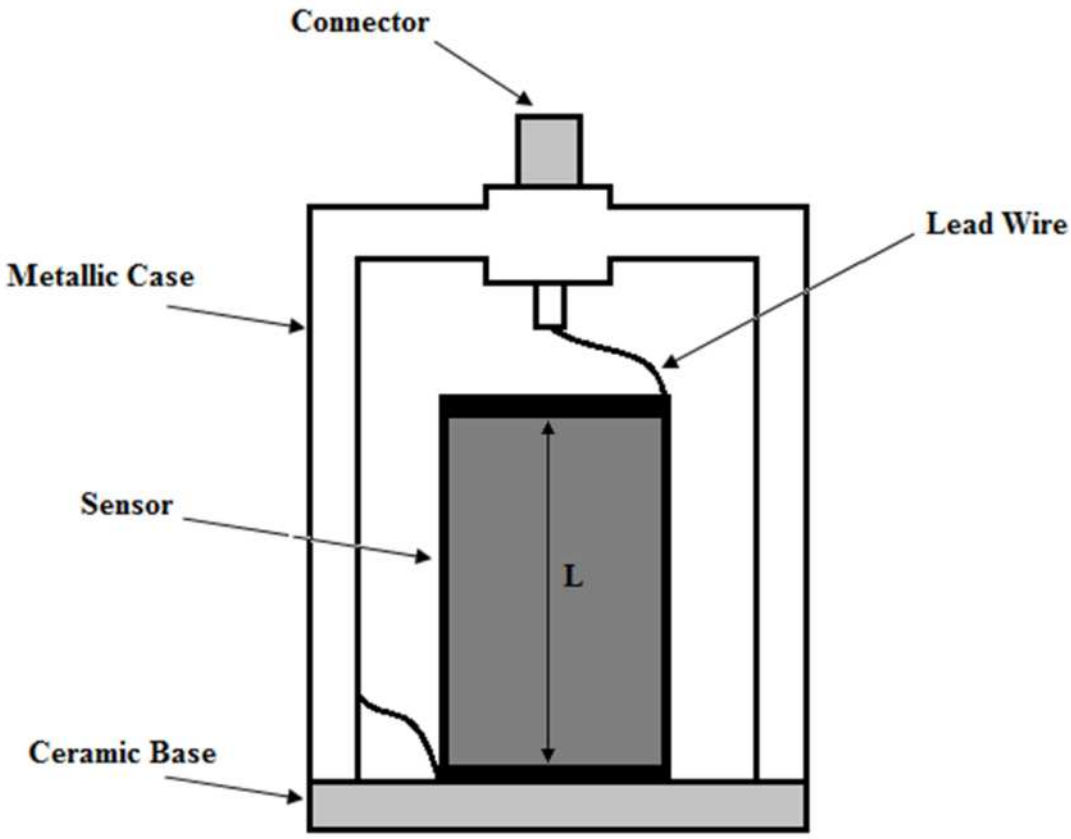


Figure 2.2. Assembly of an Acoustic Emission Sensor

defects begin to move. This movement releases energy in the form of elastic waves, which are a naturally generated ultrasound traveling through the material. The acoustic response to metal cutting may be considered as a low amplitude, continuous emission, high amplitude, or burst. During the deformation in the end milling process, there are several sources of acoustic emission [4] (see Figure 2.3).

1. Tool approach, entry, and exit.

2. Deformation of work material during cutting.

3. Chipping, breakage, and fracture of cutting inserts (or fracture of coatings in the case of coated tools).

4. Breakage and collision of chips.

5. Rubbing between chips and newly formed surface due to flank wear and chip adhesion to tool tip after considerable tool wear.

6. Multiple sources of acoustic emission in multitooth cutting.

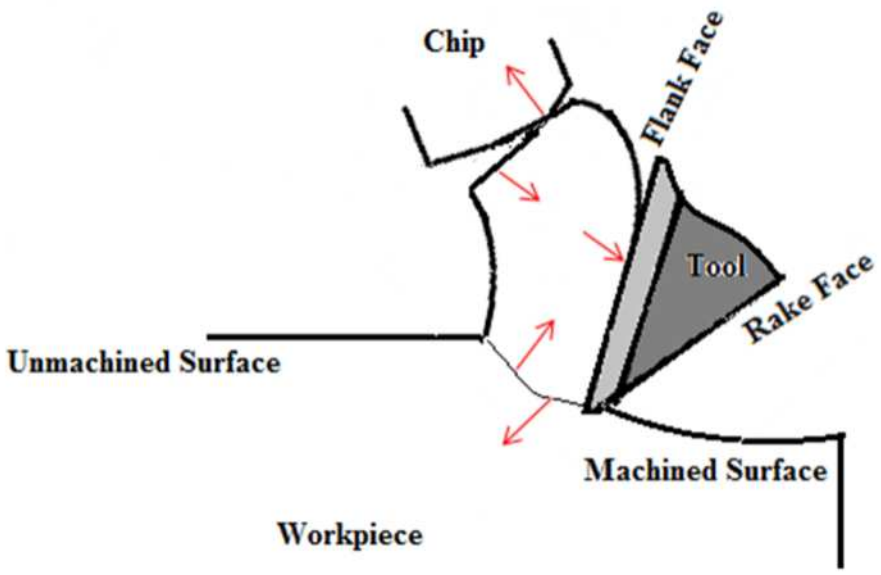


Figure 2.3. Acoustic Emission Sources During Metal Cutting and Arrows Indicate the Acoustic Emissions

The metal-cutting process generates two types of acoustic emission. Transient signals result from tool fracture, chip breakage, or collisions between chip and tool, and continuous signals are emitted by sharp or worn out tools. The continuous signals are

related to the shear that occurs in the primary shear zone and tool wear progression on the face and flank (see Figure 2.4).

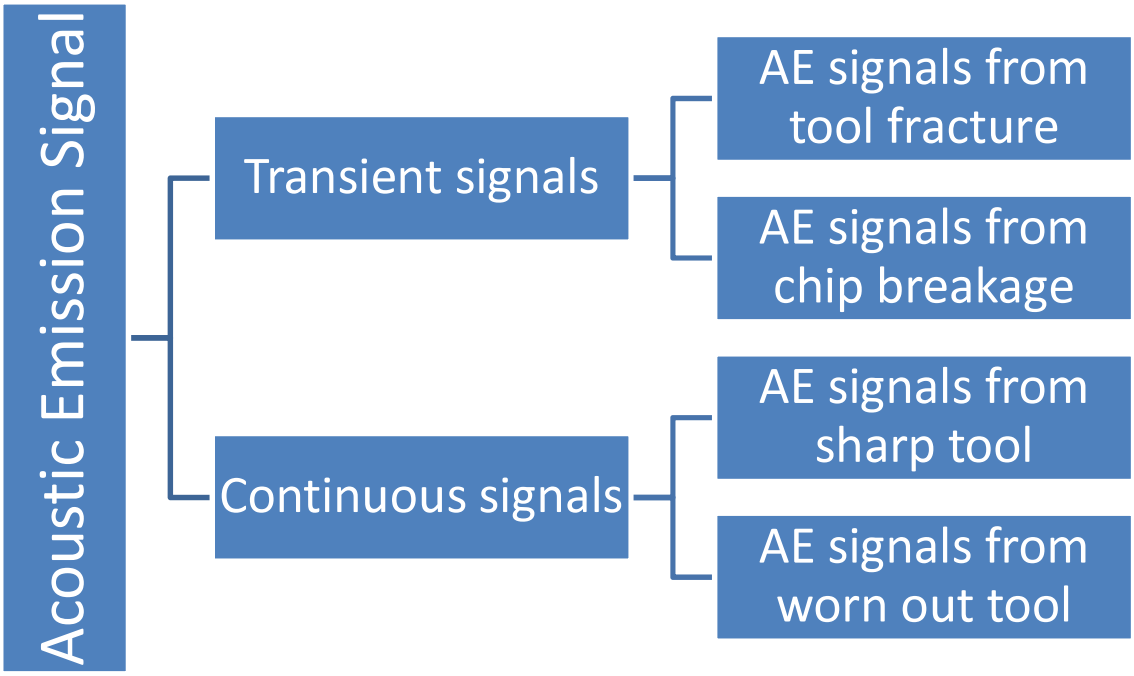


Figure 2.4. Types of Acoustic Emission in the Metal-cutting Process

2.5. FEATURES OF THE ACOUSTIC EMISSION SIGNAL

An accurate monitoring system depends on selection of the most appropriate features from sensor data and calculated characteristics for input to the system. Feature selection

can improve the output accuracy and reduce the number of features that must be collected, thus reducing costs [6]. Many features are detectable from a raw acoustic emission signal. Use of all features is not practical because irrelevant features add noise and complicate the diagnostic task. Figure 2.5 shows the parameters that can be extracted from the acoustic emission signal. They include:

- Ring-Down-Count: The number of times the signal amplitude exceeds the present reference threshold.
- Event: A microstructural displacement that produces elastic waves in a material under load or stress.
- Rise Time: The time required to reach peak amplitude from the point at which the voltage first crosses the threshold.
- Peak Amplitude: A measure related to the intensity of the source in the material producing an acoustic emission signal.
- Root Mean Square Voltage: A measure of signal energy.
- Energy Counts: The measured area under the rectified signal envelope.
- Duration: Time elapsed from the first threshold crossing to the last.

2.6. ROOT MEAN SQUARE SIGNAL ANALYSIS

The root mean square is the square root of the mean value of the squared signal. It is the alternating current voltmeter of the signal and it is always positive. The root mean square is the best way to quantify the energy created by a signal, and it is directly related to the amount of work done by the source that created the signal. It is defined as:

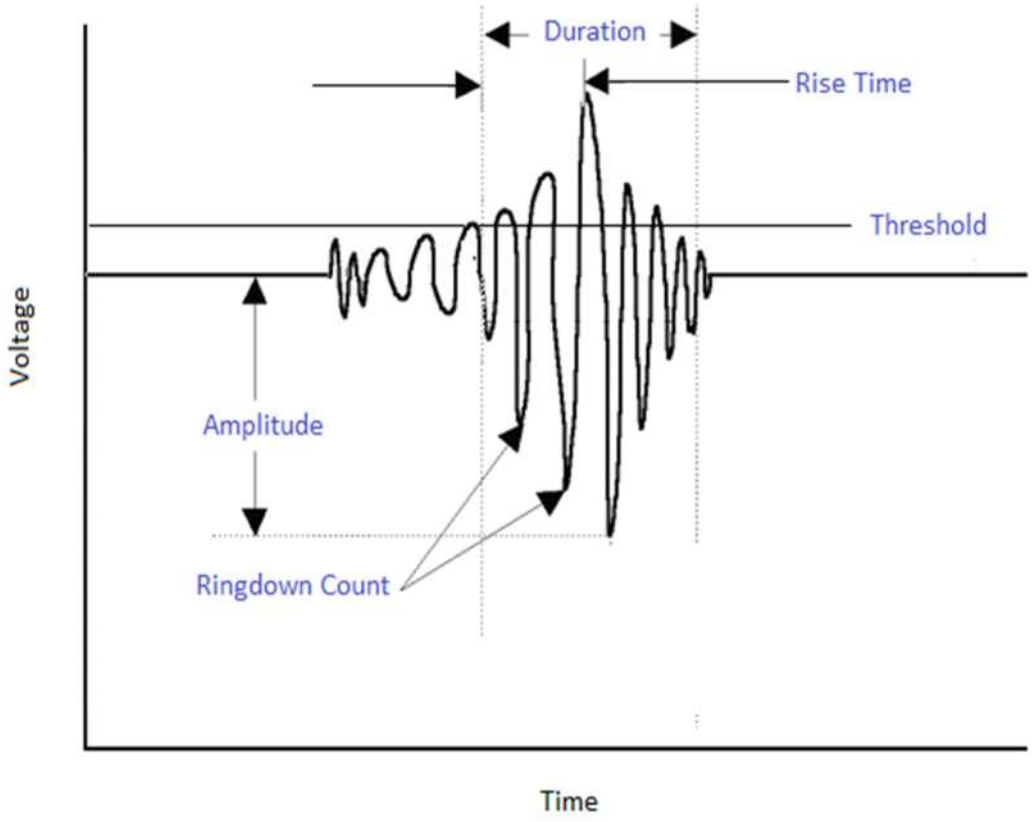


Figure 2.5. Acoustic Emission Signal Feature

$$RMS = \left[\frac{1}{\Delta T}\int_0^{\Delta T} V^2(t)dt\right] \quad (3)$$

where V (t) represents the signal function, and ΔT is the averaging time or time period.

2.7. ACOUSTIC EMISSION SIGNAL PROCESSING

A wide range of statistical signal processing methods allow data mining from discretely sampled and random acoustic emission signals. These methods include time domain analysis based on descriptive statistics such as low-order statistical moments, and frequency domain analysis based on the power spectral density (PSD) function. Such methods can be used to extract or characterize particular features of a signal. Ravindra [8] used a statistical method which is a time series modeling technique to extract parameters called *features* to represent the state of the cutting process. He studied autoregressive (AR) parameters and the power of the acoustic emission signal and AR residual signals and found them to be effective in tool condition monitoring. The power of the AR residual signal of the acoustic emissions increases with increases of the flank wear of the cutter during the turning process. Chen [9] proposed a technique based on acoustic emission signal wavelet analysis for tool condition monitoring. His method permits local characterization of the frequency band, which contains the main energy of the signals and depicts this band using wavelet multi resolution analysis. It represents the singularity of the signal using the wavelet resolution coefficient norm. Li and Yuan [10] designed a device to detect acoustic emission signals from a rotating tool. The technique involves generating features of signals from a wavelet packet transform preprocessor, then associating the preprocessor outputs with the appropriate decisions using a fuzzy clustering method (FCM). Li and Yuan used a wavelet packet transform preprocessor to decompose the signals into different frequency bands in the time domain, and the root

mean square values extracted from the decomposed signal of each frequency band were used as a feature. The features most directly related to tool wear are used as final monitoring features.

2.8. DEPTH-OF-CUT DETECTION

Controlling depth-of-cut is critical to any machining process. Any shortfall in the required depth can affect the dimensional accuracy of the part produced. Re-machining increases machining time, thus increasing costs. A reliable hybrid manufacturing management system requires that a depth-of-cut detection system be integrated with the milling machine architecture.

Many researchers have sought to control surface errors and radial and axial depth-of-cut using analytical models, simulation, force sensors, and other sensors. Choi [11] suggested an algorithm to estimate the cutting depth based on the pattern of cutting force. He found that the cutting force pattern is more useful for this purpose than its magnitude because its pattern reflects the change in cutting depth. However, magnitude is affected by a number of cutting variables, but not by the depth-of-cut.

Yang [12] suggested an analytical method to identify depth-of-cut variations based on cutting force profile features detected during end milling. Based on the profile characteristics of a single-flute, he studied end mill cutting forces and categorized them into three types. The same study categorized the cutting forces signals of both the single-flute end mill cutting and the multiple-flute end mill cutting based on the cutting process.

Wan [13] predicted the cutting forces and the surface dimensional errors using iteration schemes. Using the finite element method, he devolved a general method to

calculate static form errors in peripheral milling of thin-walled structures, and his simulation tool considered the complexity of the workpiece.

Li [14] presented a comprehensive time domain model for general end milling processes. The model measures variations in depth-of-cut using mode forms. The model can also consider additional general conditions such as cutting with a large axial depth-of-cut or small discontinued radial depth-of-cut. In addition to simulating the end milling process this method predicts a number of results for surface profiles and chatter boundaries.

Yonggang [15] examined cutting forces and categorized them into six classes according to a combination of cutting depths, and he proposed a finite-element model to study surface dimensional errors in peripheral milling of thin-walled workpieces for aerospace application. Such error prediction keeps the number of surface errors within permissible bounds.

To forecast a surface form error with the greatest efficiency and accuracy, Yonggang's model relies on a set of flexible iterative rules with a double iterative algorithm. Prickett [16] presented an approach that uses ultrasonic sensors for online monitoring of depth-of-cut during the end milling processes. The proposed monitoring process tried to contribute to the development of more efficient tool management procedures and supporting infrastructure. However, sensor resolution is an important factor limiting performance.

3. RESEARCH METHODOLOGY

3.1. INTRODUCTION

To achieve a reliable milling process management system, this work integrated a depth-of-cut detection system with the milling machine architecture using an acoustic emission sensor. The goal of the system is to operate in conjunction with an existing cutting system to provide immediate information on the current depth of the cut. The use of acoustic emission to detect depth-of-cut relies on the fact that the deformation of a material is accompanied by dissipation of energy in the form of acoustic waves, which can be detected by piezoelectric sensors mounted on the surface of the component or on the fixture. The system does not attempt to measure the dimensions of the workpiece online. The objective of this study is to develop a depth-of-cut detection system during an end-milling cutting operation.

Due to the inherent complexity and variability of machining mechanisms, the characteristics of the sensor signal obtained in machining processes can be complex in terms of both nonlinearity, and nonstationarity. To overcome this complexity, the present work used the multiple regression model to represent the relationship between the acoustic emission signal and depth-of-cut. The output of the sensor and data of cutting conditions and tool status are fed to a regression model to measure operation quality during machining. After the model was calibrated, the inference system estimated the depth-of-cut in real time from the experimental sensor signal and the cutting conditions. The results of the monitoring algorithm can warn the operator to take the corrective actions to reach the required depth-of-cut. The difference between the desired depth-of-

cut and the actual depth-of-cut may be a result of incorrect workpiece set-up, tool length offset change (tool wear), or irregularity of workpiece dimensions. Previous manufacturing processes may also lead to errors in depth-of-cut. For example, when a workpiece is manufactured by laser deposition, forging, or casting, the dimensions are not always accurate and uniform.

3.2. ACOUSTIC EMISSION SYSTEM

The acoustic emission system used here was made by Kistler and consists of an acoustic emission sensor (shown in Figure 3.1.) and acoustic emission coupler type 8152B111. The acoustic emission sensor is made up of the sensor housing, a piezoelectric sensing element, and a built-in impedance converter. The sensing element, made of piezoelectric ceramic, is mounted on a thin steel diaphragm. Its construction determines the sensitivity and frequency response of the sensor. The coupling surface of the diaphragm welded onto the housing is slightly obtruded to measure the acoustic emission signals. Thus, a precisely defined coupling force results when the sensor is mounted, assuring a constant coupling for the acoustic emission transmission. The sensing element is acoustically isolated from the housing by design and therefore well protected against external noise. The Kistler acoustic emission sensors are highly sensitive to surface and longitudinal waves over a broad frequency range.

The AE-Piezotron coupler shown in Figure 3.2 comprises plug-in modules that process the raw signal and transfer it to a root mean square. The main function of the coupler is to supply power to the sensor and process the sound emission signal. The gain factor, low and high pass filters, and integration time constant are included in one

electronic board, allowing the best possible adaptation to a specific monitoring function. The coupler provided 0–5 V root mean square voltage signals proportional to the measured depth-of-cut and eliminated any need for further signal processing. Figure 3.3 shows the coupler assembly diagram.

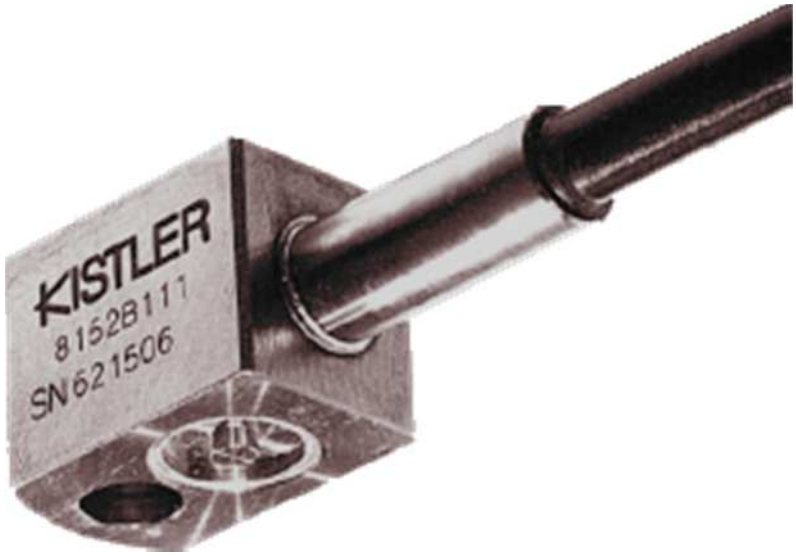


Figure 3.1.Kistler 8152B111 Acoustic Emission Sensor



Figure 3.2. Piezotron Coupler

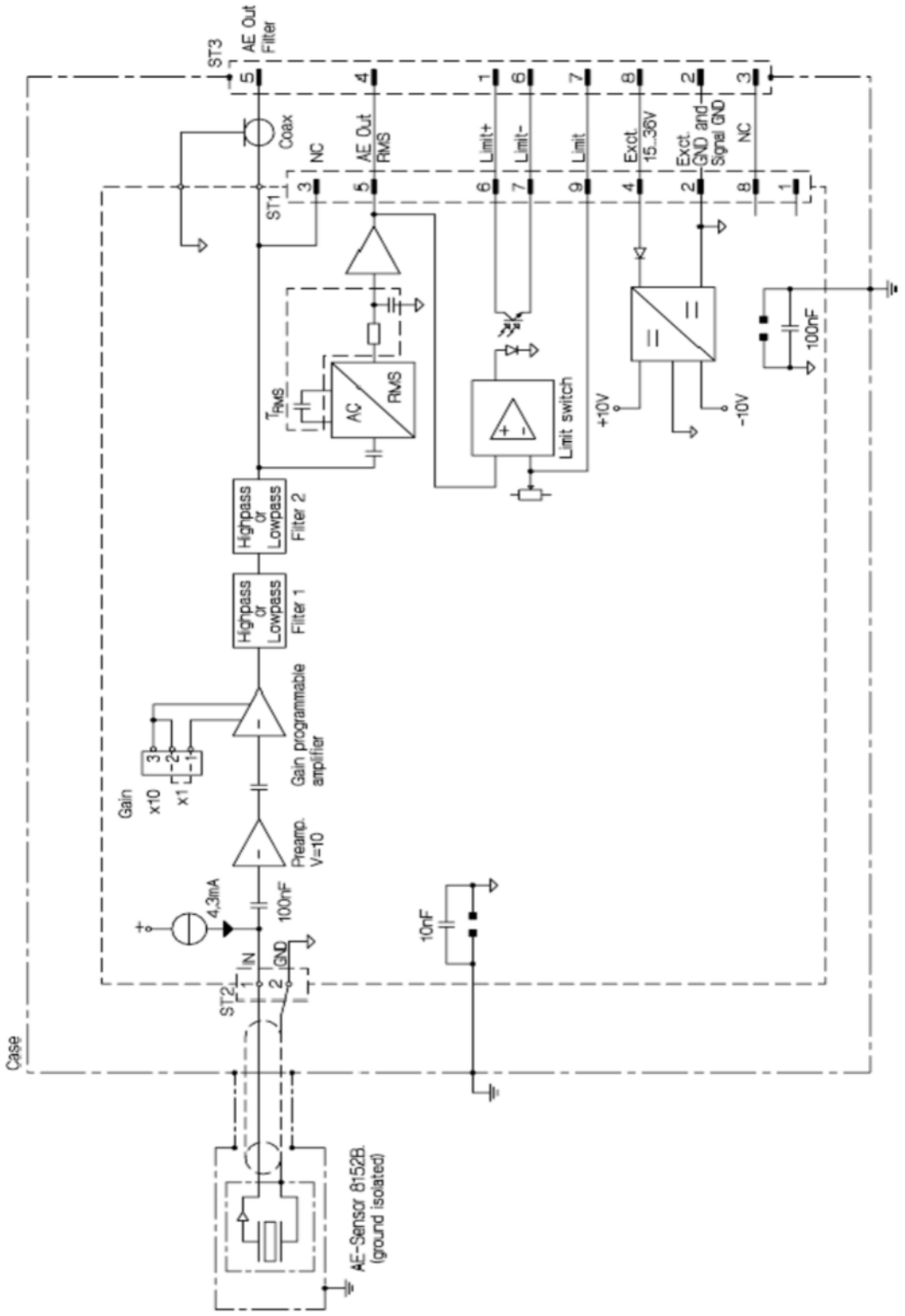


Figure 3.3. The Coupler Assembly Diagram

3.3. EXPERIMENTAL SETUP

Figure 3.4 shows a schematic diagram of the experimental set-up. The milling process was carried out on a Fadal vertical 5-Axis computer numerical control machine (3016L) using a carbide flat-end mill (0.5 in) to cut deposited stainless steel 316 workpieces. The control interface (National Instrument PXI 7240 and PXI 1250) provided the control and data acquisition. An acoustic emission sensor (Kistler 8152B211) captured a high-frequency signal. The bandwidth of the AE sensor was 10 to 1000 kHz. The RMS signals were first fed through the data acquisition system and then recoded and processed using Labview software. A 500X digital microscopic camera was used to detect tool status without disengaging the tool from the tool holder. The tool condition was documented from the bottom edge radius, which was measured in place with the aid of the vision system.

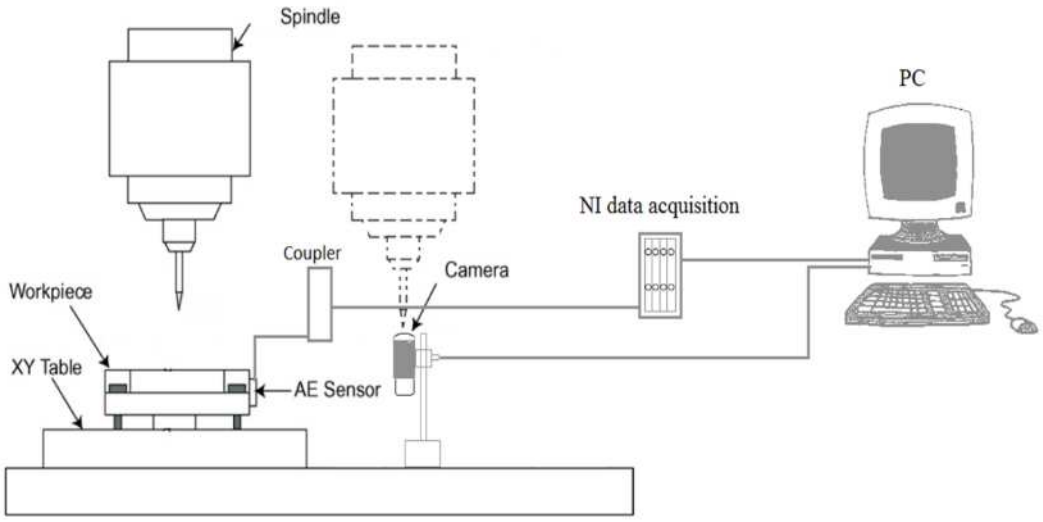


Figure 3.4. Experimental Setup

3.4 TOOL STATUS CATEGORIZATION

This study classified tool status according to tool life or tool wear, which is caused by progressive loss of tool material during cutting and which thus changes the shape of the cutting edge. Image J software was used to convert tool wear from a pixel scale to micrometer scale. Once the measuring scale was calibrated, tool wear was measured by counting pixels from the vision system and comparing the number with the scale on the reticle. Figure 3.5 shows tool wear of a four-flutes 0.5 inch end mill.

The international organization for standardization [20] recommends that the tool be considered worn-out and reached its end point at 0.3 mm, or 300 μm. Here, the output was assigned a value of 1 (for a fresh tool with wear less than 130 μm), 2 (for an average tool between 130 μm and 300 μm), or 3 (for a worn-out tool with wear greater than 300 μm). Figure 3.6 shows a fresh tool with 10 μm tool wear and Figure 3.7 shows a worn-out tool with 320 μm tool wear. In both cases, the tool has four flutes with a different level of wear, so the tool wear value represents an average.

The three tool wear categories were established based on the tool life curve (Taylor tool life curve) which divides the tool life into three stages or regions, initial, progressive, and severe (see Figure 3.8).

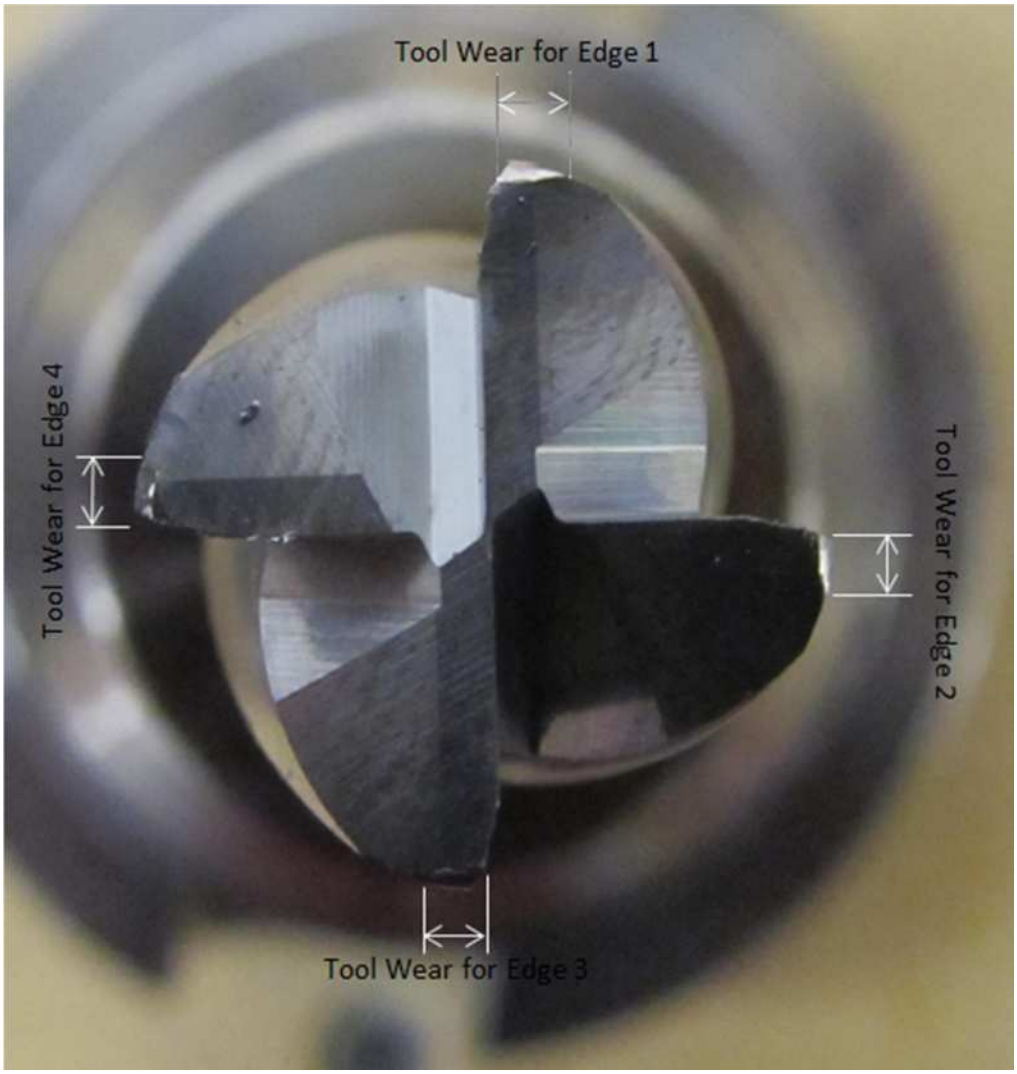


Figure 3.5. Tool Wear for 0.5 Inch End Mill

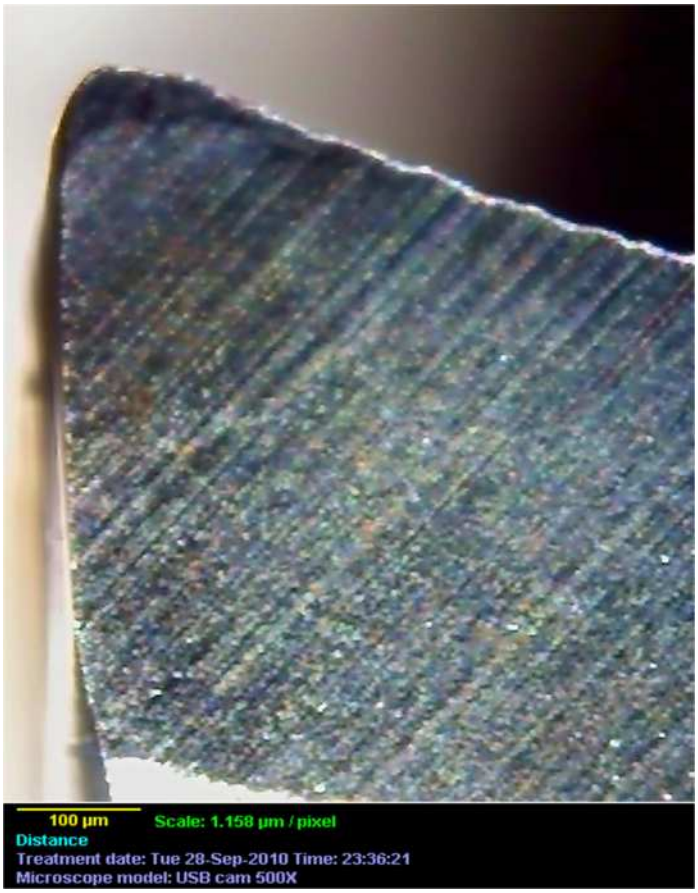


Figure 3.6. Fresh Tool (The Wear = 10 µm)

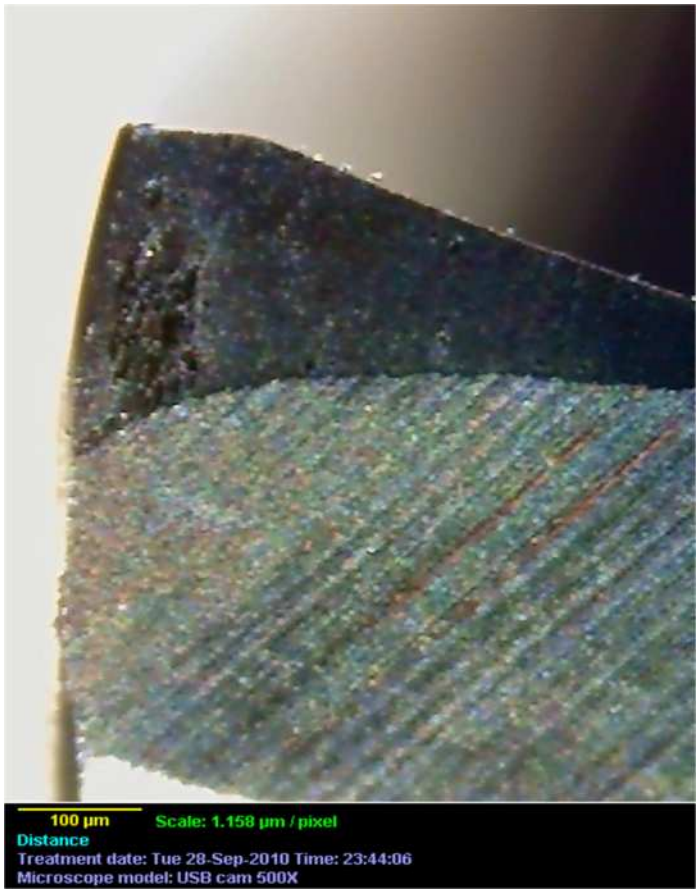


Figure 3.7. Worn-out Tool (The Wear = 320µm)

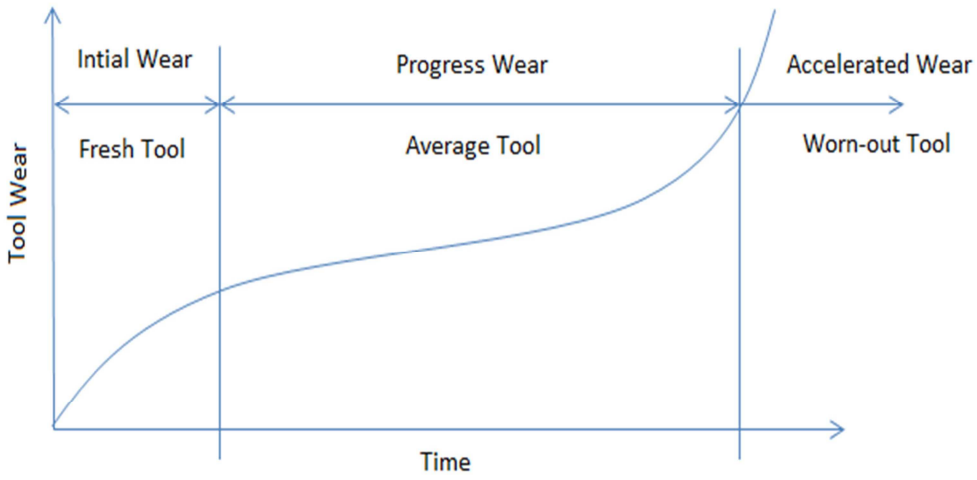


Figure 3.8. Typical Taylor Tool Wear Curve

4. ANALYSIS AND MODELING

4.1. THE RAW ACOUSTIC EMISSION SIGNAL

Figure 4.1 shows the acoustic emission signal acquired during an axial slot milling. The cut passes through three different regions, the engagement region, the steady cut region, and the disengagement region. This study considered only steady cutting in the analysis and molding. In the engagement and disengagement regions, the root mean square value was higher than the average of the signal. The engagement and disengagement time were calculated as follows:

$$T\ (\text{Sec}) = D \times 60/(2 \times F) \qquad (4)$$

where D is the tool diameter (mm) and F is the Feed rate (mm/min). For example, when the tool diameter was 0.5" (12.7 mm), the feed rate was 100 mm/min, as in runs 1, 6 and 7:

$$T\ (\text{Sec}) = 12.7 \times 60/(2 \times 100) = 3.81\ Sec.$$

Figure 4.2 shows the percent engagement against the root mean square signal, and the moving average. As the engagement increased, the acoustic emission signal increased. This phenomenon was a result of the friction at the cutting edge and a 90° lead angle, which caused high radial cutting forces and high entry shock load. This dramatic

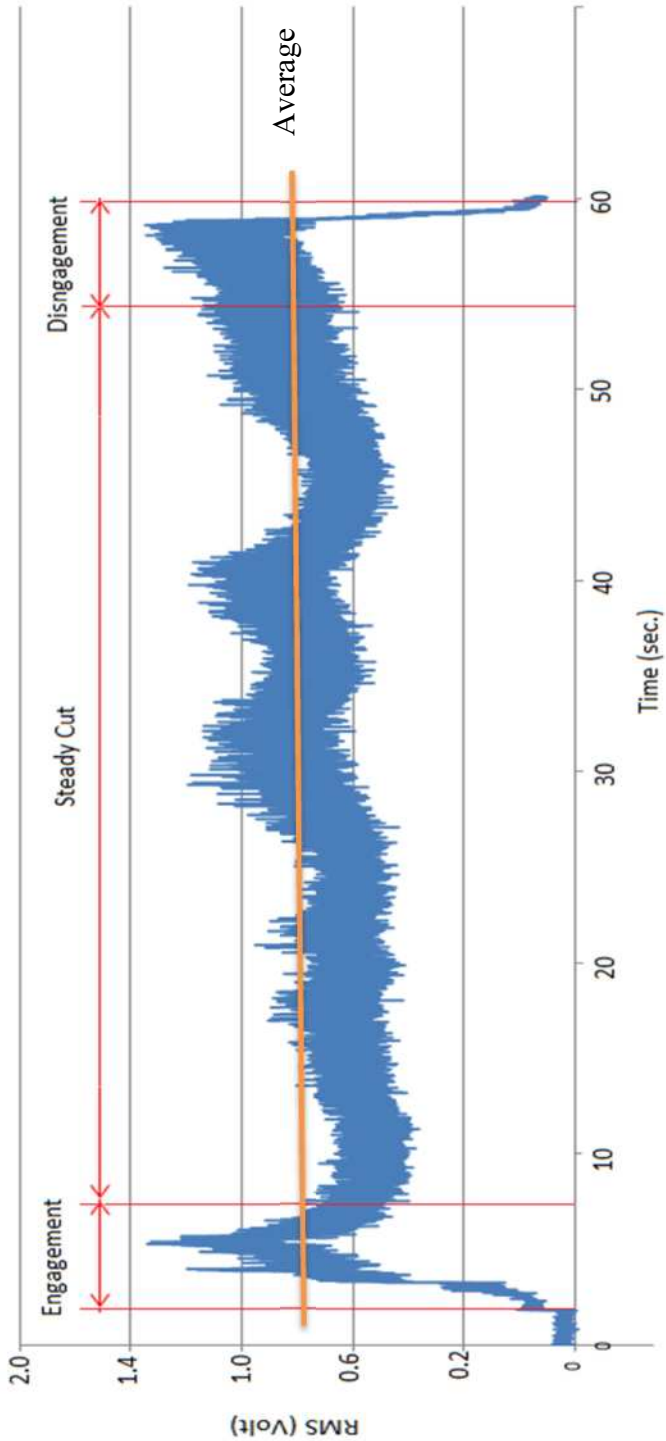


Figure 4.1. The Raw signal (2 mm depth of cut, 5500 RPM spindle speed and 100 mm/min feed rate)

increase in signal was also a result of the chip thickens; when the cutter diameter was approximately equal to the width of the cut, as shown in Figure 4.3, the chip was very thin at the entrance and exit of the cut. Thin chips cannot carry away as much heat as thicker chips; therefore, the heat is transferred back into the insert, causing premature edge failure chatter. The same phenomenon occurs when the tool exits the part, but in reverse, as shown in Figure 4.4.

4.2 MOVING AVERAGE AND SPIKES REMOVAL

Transient signals, which can be seen as spikes in the oscilloscope, are a result of tool fracture, chip breakage, or collisions between chip and tool. These spikes should be removed to ensure unbiased calculations and representation of the statistical properties of the signal. The spikes are values in the acoustic emission signal that do not follow the same distribution as the majority of signal values or do not fall within an interval defined by upper and lower bounds. This research, assumed that the root mean square values follow a normal distribution, and use three standard deviations as control limits is effective in eliminating the spikes. The upper and lower boundary limits are defined by the formula $(\bar{x} \pm 3\sigma)$, where $\bar{x}$ is the average of the root mean square, and σ is the standard division of the root mean square for n time window. Any point outside these limits is replaced by the preceding value, and the moving average is then used to smooth out short-term fluctuations and highlight long-term signal trends. Figure 4.5 shows the results of the algorithm and original signal.

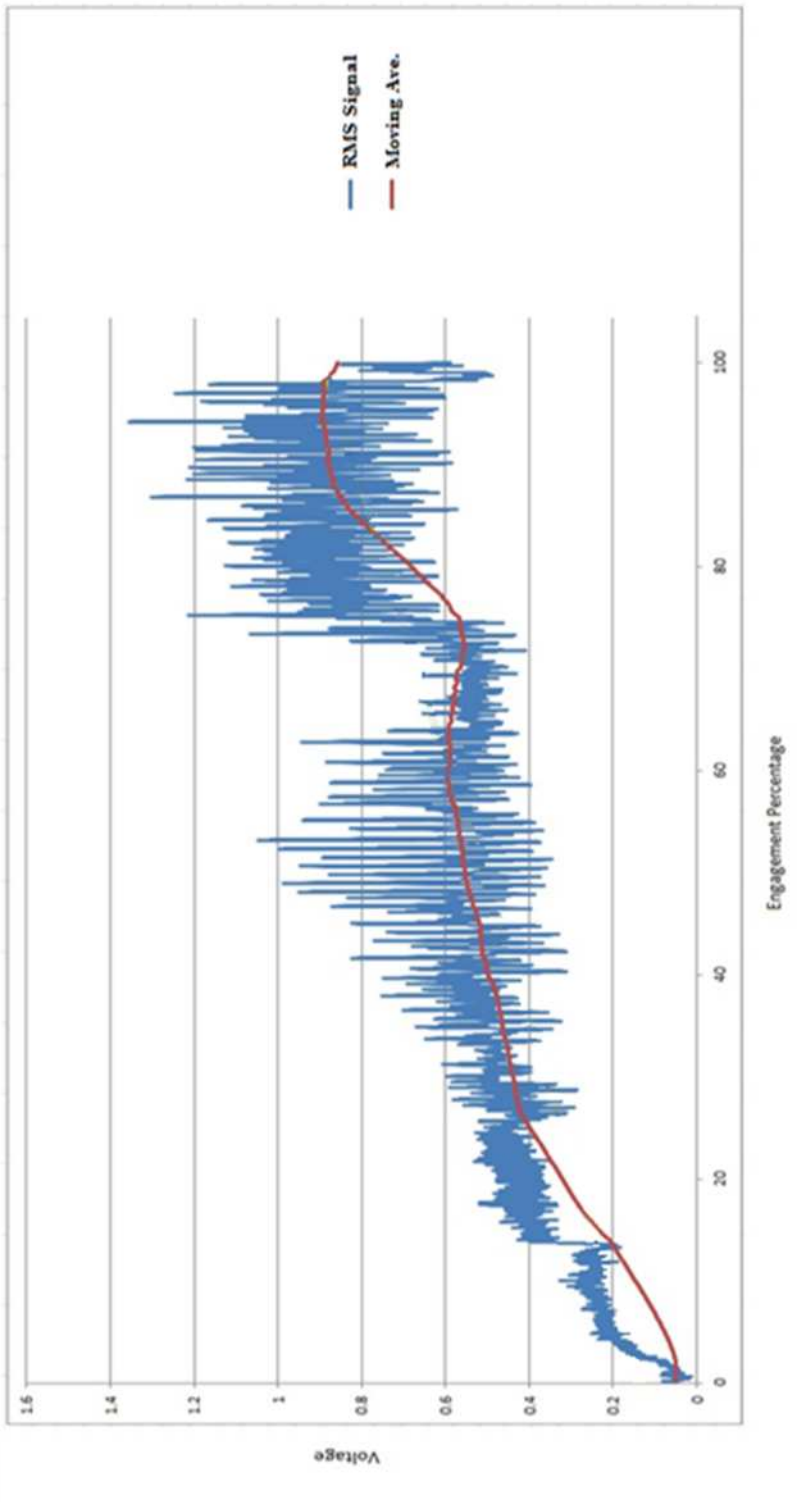


Figure 4.2. Root Mean Square at the Engagement Region



Figure 4.3 Axial Slot Milling

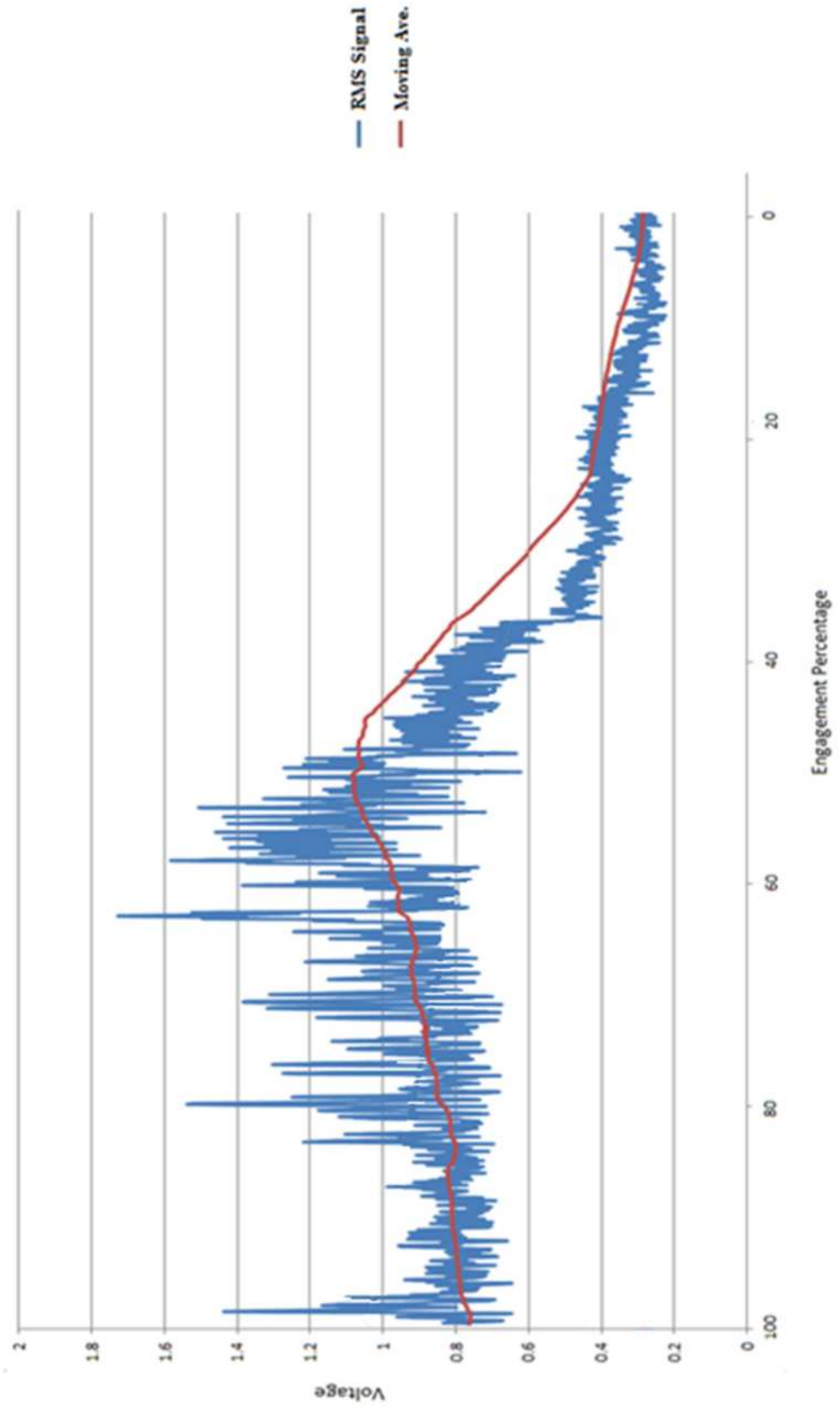
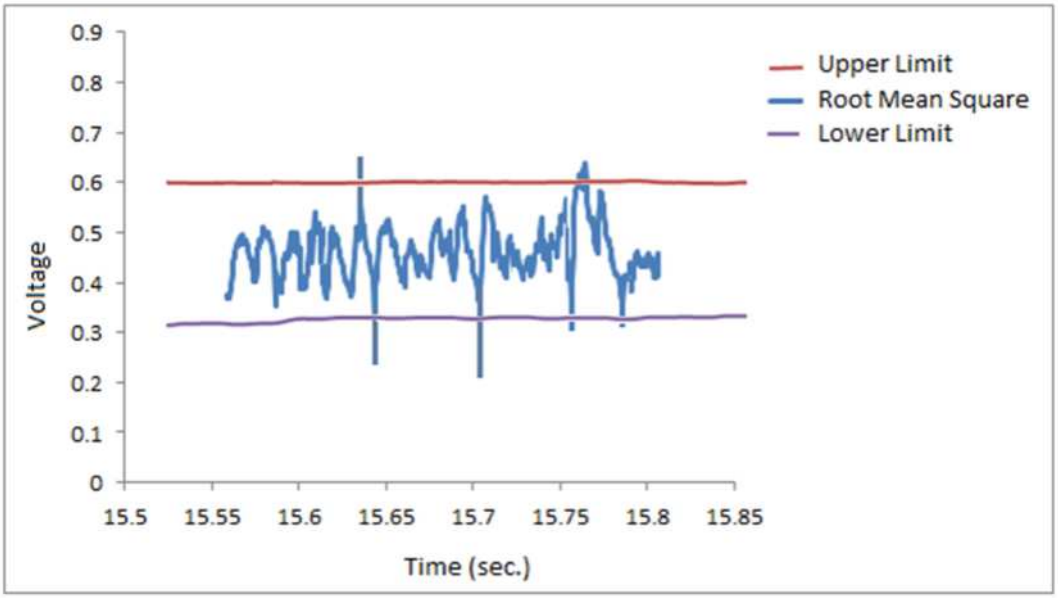
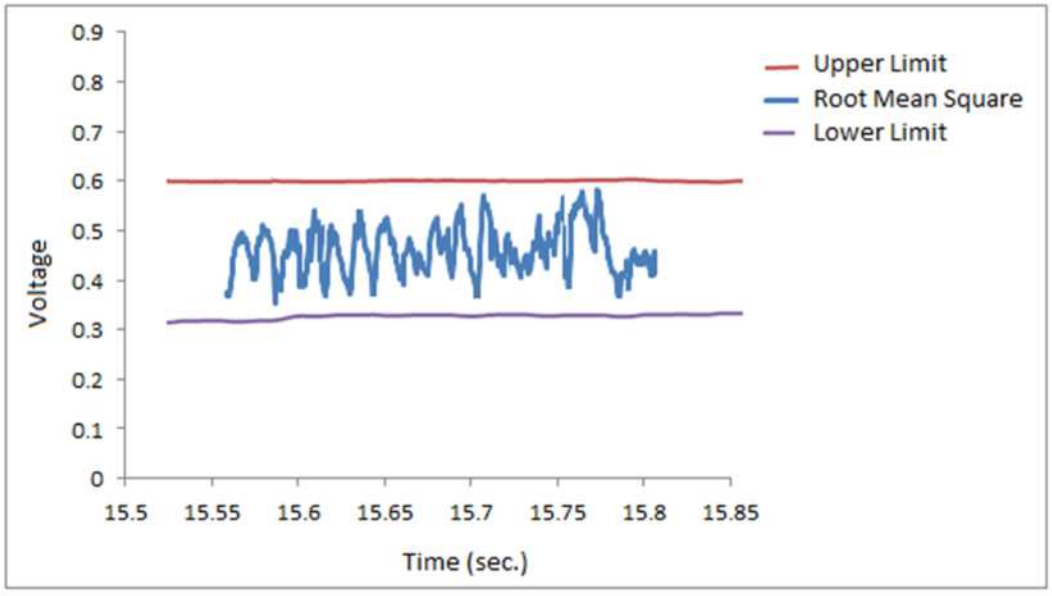


Figure 4.4. Root Mean Square at Disengagement Region



(a)



(b)

Figure 4.5 Acoustic Emission Signal (a) Original (b) after Removal of Spikes

4.3 THE ACOUSTIC EMISSION SIGNAL SENSITIVITY TO DEPTH-OF-CUT CHANGES

Figure 4.6 shows the change in the acoustic emission signal caused by a change in the depth-of-cut. It denotes a sequence of three cuts through the workpiece performed at three different depths (0.5, 1.5, and 2.0 mm) at a feed rate 70 mm/min and a cutting speed 3000 RPM with fresh tool. The signals were acquired separately for each depth-of-cut; they are presented in one figure to show the sensitivity of the acoustic signal to the changes in depth-of-cut. The transition between the depths divides the figure into three zones. The x-axis represents the cutting time, and the y-axis represents the signal voltage. There is excellent correlation between the acoustic emission signal and the changes in depth-of-cut, as the depth-of-cut increases as the root mean square of the signal increases.

4.4. DESIGN OF EXPERIMENTS

Most research has focused on the use of a force signal to detect, model, and control radial depth-of-cut and chip thickness [11-15], but no study has used an acoustic emission sensor to predict axial depth-of-cut during end milling. The experiments described here were designed to identify the most significant factors affecting the acoustic emission signal during the end milling process. Therefore, their outcomes are significant for the computation of depth-of-cut, and the model considers the cutting tool condition and the cutting variables.

The factors were selected based on work done by Dornfeld [21], who developed a model describing acoustic emission based on the assumption that the power of acoustic emission signal is related to the power that produces plastic deformation. Most cutting operations

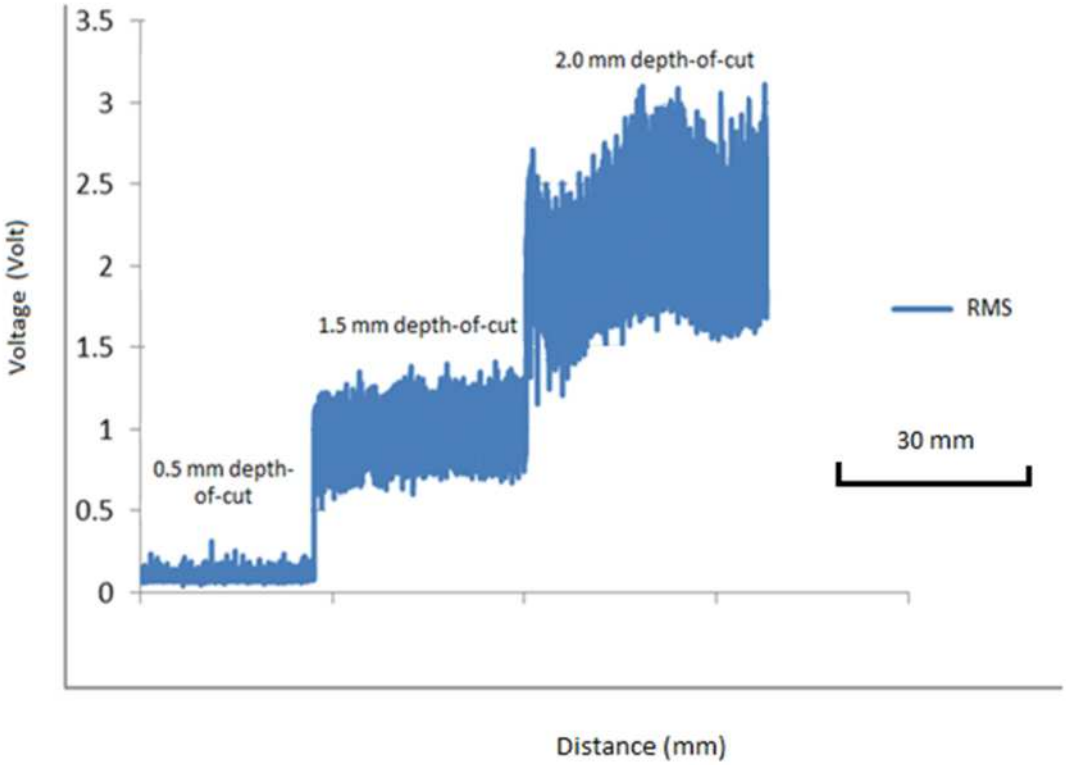


Figure 4.6 Acoustic Emission Sensitivity to the Depth-of-cut Changes

are three-dimensional and orthogonal cases are often encountered, including surface broaching and certain turning and milling operations. The model is limited to the orthogonal cutting process and can be expressed as

$$AE_{rms} = C_1 \sin\alpha \left[\tau_k a_p U \left(\frac{\cos\alpha}{\sin\emptyset\cos(\emptyset-\alpha)} t_1 + \frac{(l-2l_1)\sin\emptyset}{3\cos(\emptyset-\alpha)} + C_2 W\right)\right]^{\frac{1}{2}} \quad (5)$$

where AE_{rms} is the root mean square of the acoustic emission signal, α is the rake angle, $\emptyset$ is the shear angle, τ_k is the shear strength of the workpiece material, a_p is the width of cut (axial depth-of-cut), U is cutting velocity, l is chip-tool contact length, l_1 is the length of the sticking zone, t_1 is the feed load, W is the average flank wear and C_1 and C_2 are signal attenuation. Here, the root mean square is proportional to the square root of the cutting speed.

Dornfeld assumed that α and τ_k are constant. The value of l_1 is approximately one-half the measured contact length, and $\emptyset$ must be determined experimentally; it can be assumed to be constant for the same tool geometry. Thus, equation 5 can be simplified as

$$AE_{rms}^2 = K_1 a_p F + K_2 a_p N + K_3 a_p N\, W \qquad (6)$$

where N is the cutting speed, which is equal to U/ (π × tool diameter), and F is the feed rate (t_1× N × number of flutes). The constants K_1, K_2, and K_3 depend on the tool geometry and workpiece material; they were identified by applying factorial design to the main factors affecting the acoustic emission signal at various cutting depths (see Table 4.1). These factors include depth-of-cut, spindle speed, feed rate, and tool status

Using the Taguchi L_9 (3^4) experimental design with three replications, a total of 27 cutting tests were run randomly, and a range of cutting variables was collected, as shown in Table 4.2.

Table 4.1 Factors and Levels Defined for Experimentation

Depth of Cut(mm)	Cutting Speed (RPM)	Feed Rate (mm/min)	Tool Status
0.5	1500	40	≤130 µm
1.0	3000	70	> 130 µm and ≤300 µm
2.0	5000	100	> 300

Table 4.2. Taguchi L_9 (3^4) Experimental Design

Experiment	Depth of Cut (mm)	Cutting Speed (RPM)	Feed Rate (mm/min)	Tool Status	Average RMS
1	1	1	1	1	0.556422
2	1	2	2	2	0.102253
3	1	3	3	3	0.304408
4	2	1	2	3	0.153831
5	2	2	3	1	0.300762
6	2	3	1	2	0.321306
7	3	1	3	2	0.088805
8	3	2	1	3	0.211103
9	3	3	2	1	0.117241

This model was developed using MINTAB statistical software, with four independent variables: feed rate, cutting speed, tool status, and the depth-of-cut. The dependent variable was the squared root mean square of acoustic emission signal. Although this research is sought to estimate depth-of-cut, the data were used to model the squared root mean square.

The dimensions of the workpiece were 2x2x4 in; they were designed to allow the machining of three replicates, each 4 inches long. Figure 4.7 shows the geometry of the workpiece. The design of experiments included the following steps:

1. Run a set of experiments with a fresh cutting tool, and record the acoustic emission signal.

2. Wear the cutting tool until it reaches an average tool wear (just above 130 μm) consistent with the predetermined tool status criteria.

3. Run a second set of experiments with a tool with average wear, and record the acoustic emission signal.

4. Wear the cutting tool until it is a worn-out (just above 300 μm).

5. Run the last set of experiments with a worn-out tool, and record the acoustic emission signal.

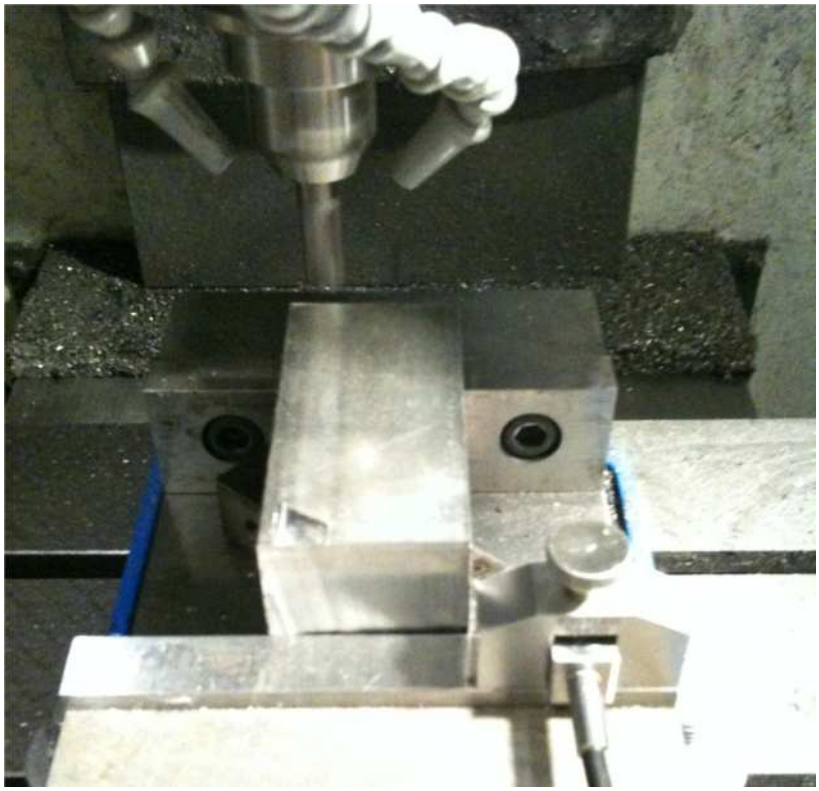


Figure 4.7. Workpiece Geometry

5. RESULTS AND DISCUSSION

5.1. STATISTICAL RESULTS OF EXPERIMENTAL DATA

To assess linearity, figure 5.1 plots the residuals on the vertical axis against the corresponding squared root mean square values on the horizontal axis. The fitted model is appropriate for representing the data because there is no obvious pattern in the plot, and the residuals are spread fairly evenly above and below 0 for the differing values of squared root mean square, indicating random variation of the residuals around the mean value.

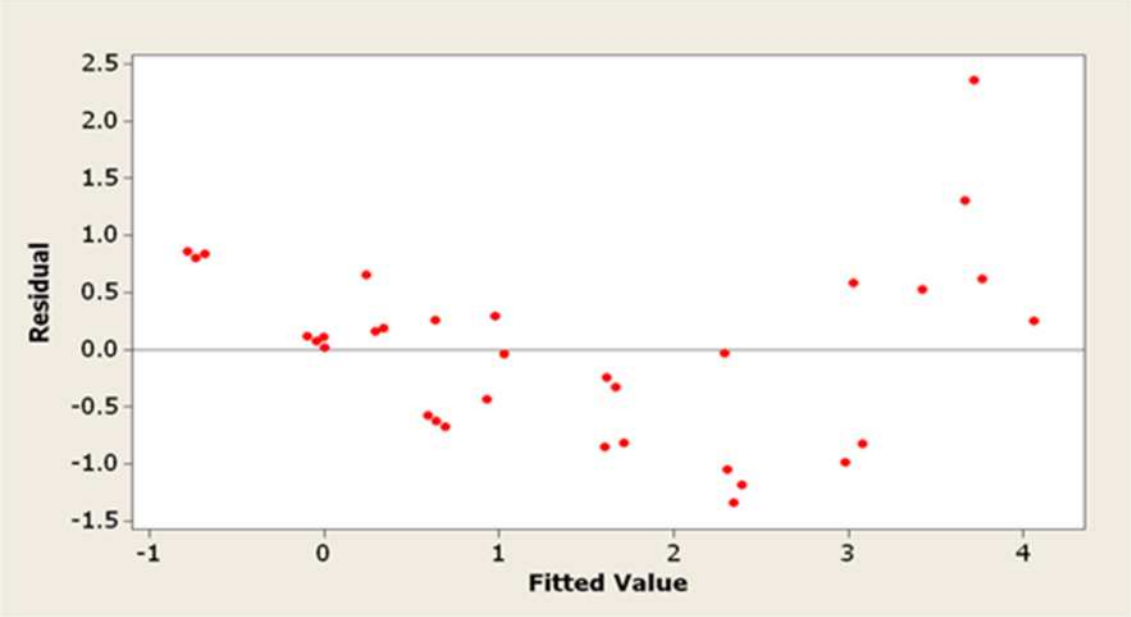


Figure 5.1. Residual Plot for the RMS^2

Figure 5.2 evaluates the assumption of that the errors are independent by plotting the residuals in the order in which the data were collected. Data collected during the experiment do not exhibit an autocorrelation effect among successive residuals. If this relationship existed (which would violate the assumption of independence), it would be apparent in the plot of the residuals versus the order of data collected.

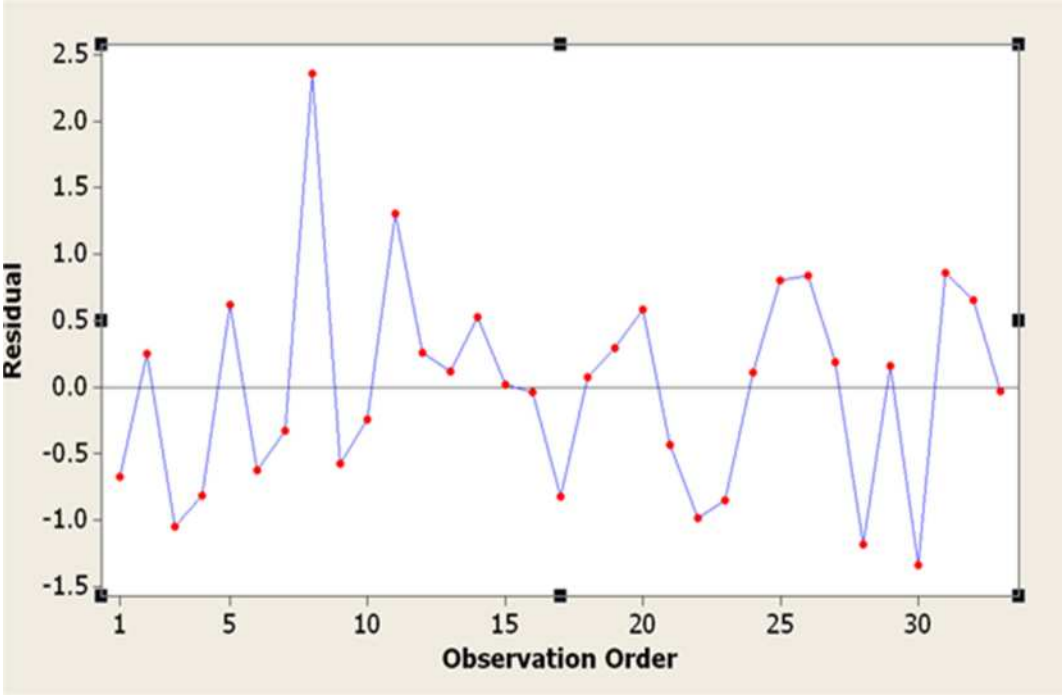


Figure 5.2. Order Plot of the Residuals

The normal probability plot in figure 5.3 determines whether the residuals follow a normal distribution. The data skew neither to the left nor to the right, and the residuals are identically and independently normally distributed.

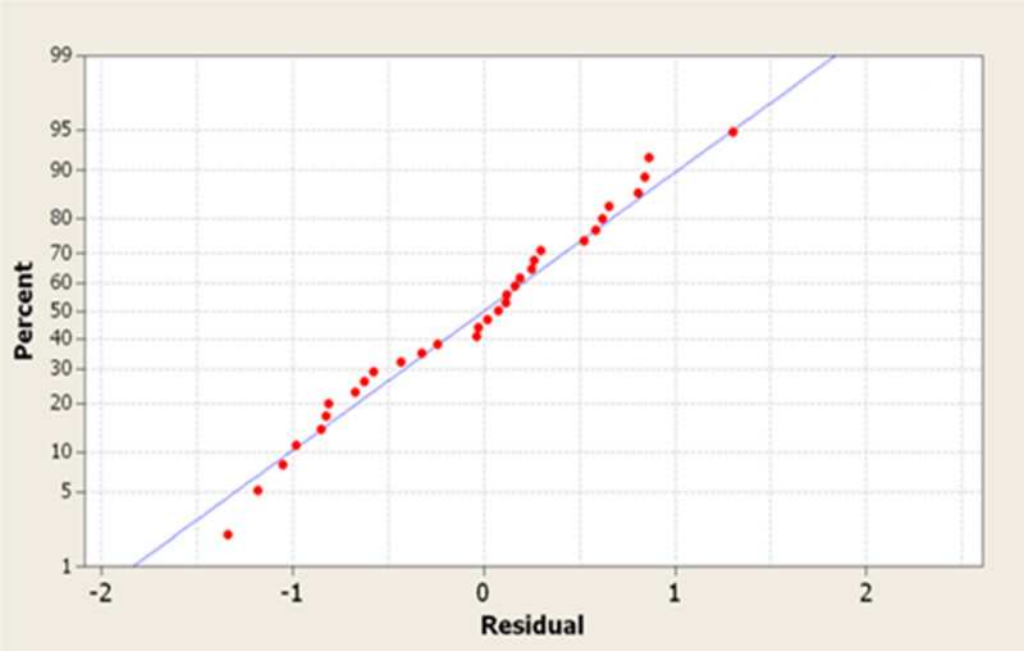


Figure 5.3. Normal Probability Plot of the Residuals

The analysis of variance shows that the coefficient of determination is equal to 0.8716, therefor, 87.16 % of the variation in RMS^2 is explained by the variability in the regression model, and the interaction among axial depth-of-cut, cutting speed, and tool

status is significantly greater than the other two interactions, in where the P-value in zero. However, the interaction between axial depth-of-cut and feed rate is less significant, with a P-value 0.358.

5.2. ESTIMATED RMS^2

Using regression analysis, the constants K_1, K_2, and K_3 deposited stainless steel 316 were determined to be 0.00590, 0.000583, and 0.000192, respectively. Figure 5.4 shows the actual outputs (RMS^2) versus the outputs obtained from the regression model. There is close agreement between the actual and the estimated values.

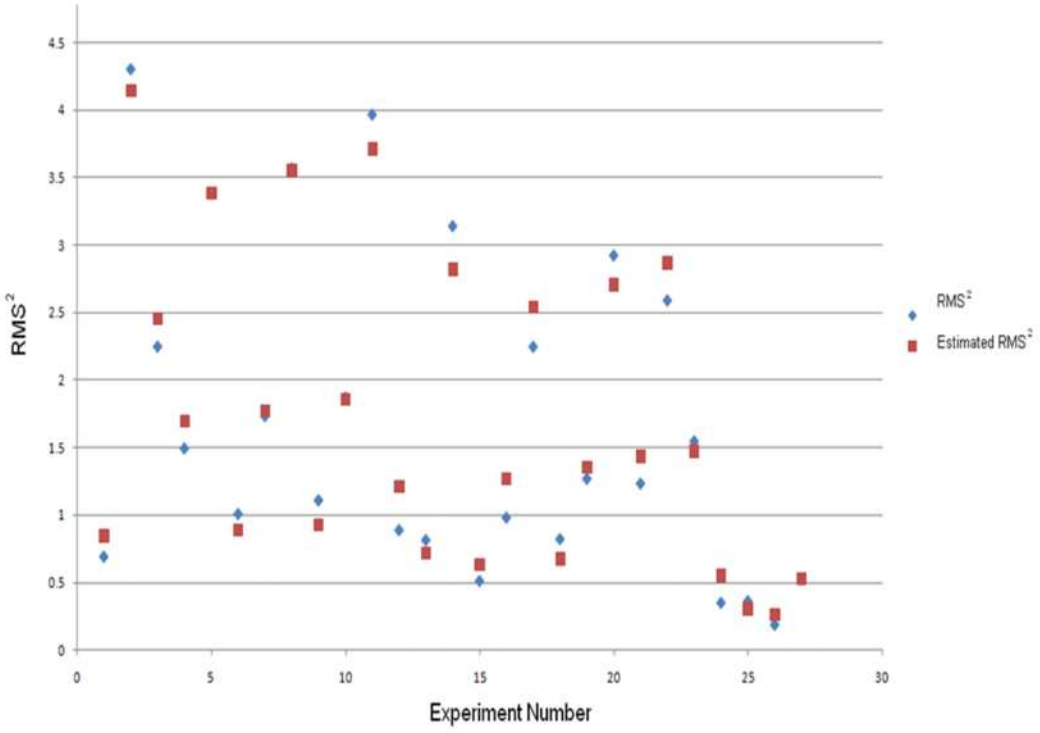


Figure 5.4. Estimated RMS^2 vs. Actual Values

5.3. ESTIMATION OF DEPTH-OF-CUT

Depth-of-cut can be estimated from the model in equation 6 as follows:

$$a_p = \frac{AE_{rms}^2}{K_1 F + K_2 N + K_3 N\, W} \qquad (7)$$

thus, the depth-of-cut of deposited stainless steel 316 can be calculated as follows:

$$a_p = \frac{AE_{rms}^2}{0.00590\, F + 0.000583 N + 0.000192 N\, W}.$$

Figure 5.5 shows the depth-of-cut estimated at 2 mm, 1 mm, and 0.5 mm with a feed rate of 40 mm/min and a cutting speed of 5000 rpm. Clearly, the system can detect the depth-of-cut with a maximum acceptable error of approximately 0.25 mm. The accuracy of depth-of-cut estimation depends on the quality of the acquired signal.

This work tested the efficiency of the model in estimating depth-of-cut in an interrupted cutting process. As shown in Figure 5.6, a 25.2 mm slot was made in the workpiece perpendicular to the machining direction. The depth-of-cut was 1 mm, the cutting speed was 4000 rpm, the feed rate was 30 mm/min, and the tool was fresh. 51 second is the time required for the tool to cross the gap (25.2/30), and 25 second is both engagement and disengagement time subtracted from 51 seconds. Figure 5.6 shows that the model is able to distinguish the slot; thus the system is capable of detecting the

engagement and the disengagement of the tool with the workpiece as well as the depth-of-cut.

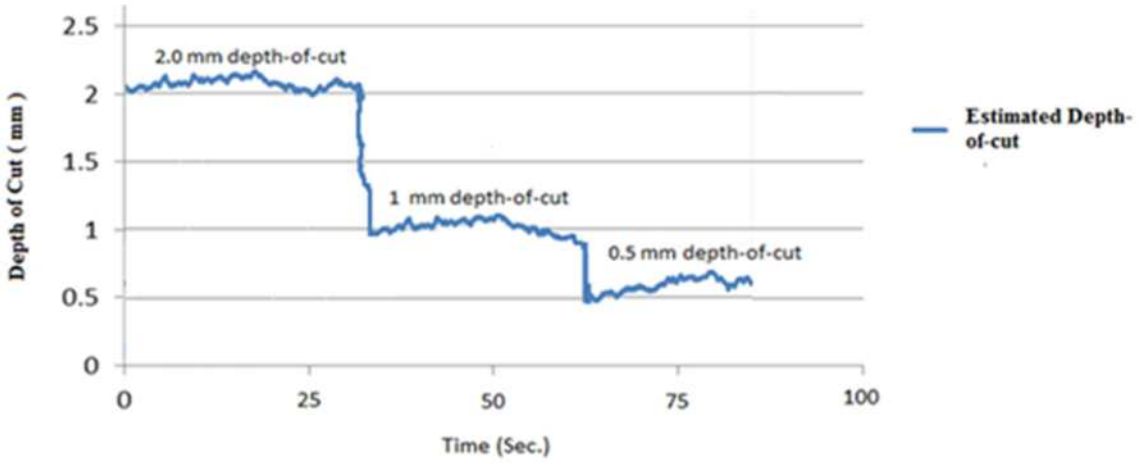


Figure 5.5. Depth-of-cut Estimation

Figure 5.7 shows both the nominal and estimated depth of cut for inclined surface cutting. A 10 mm ramp was created at the end of 60 mm cutting with 2 mm height as shown in the cutting geometry in the figure. The cutting speed was 4000 rpm, the feed rate was 30 mm/min, and the tool was fresh.

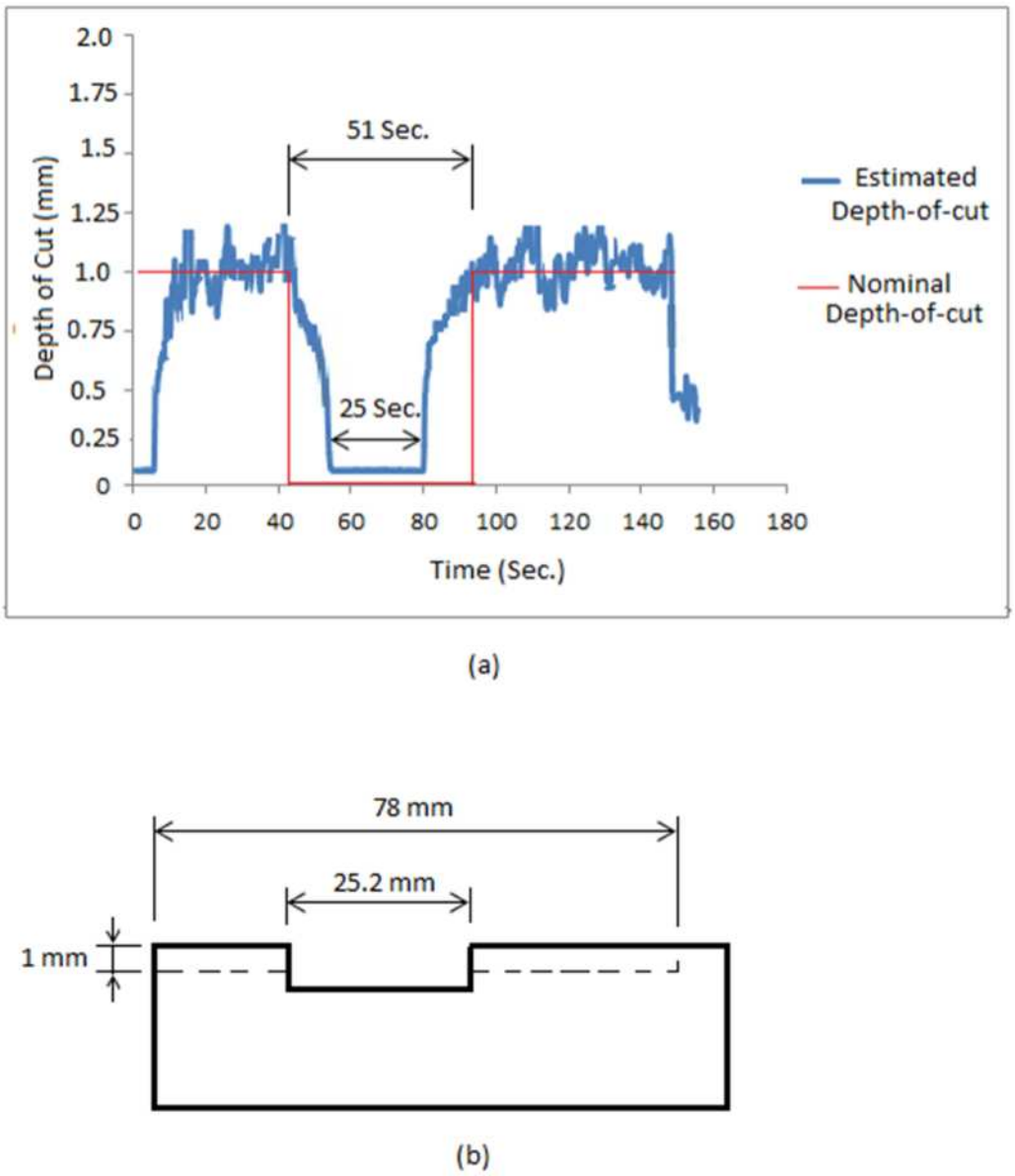
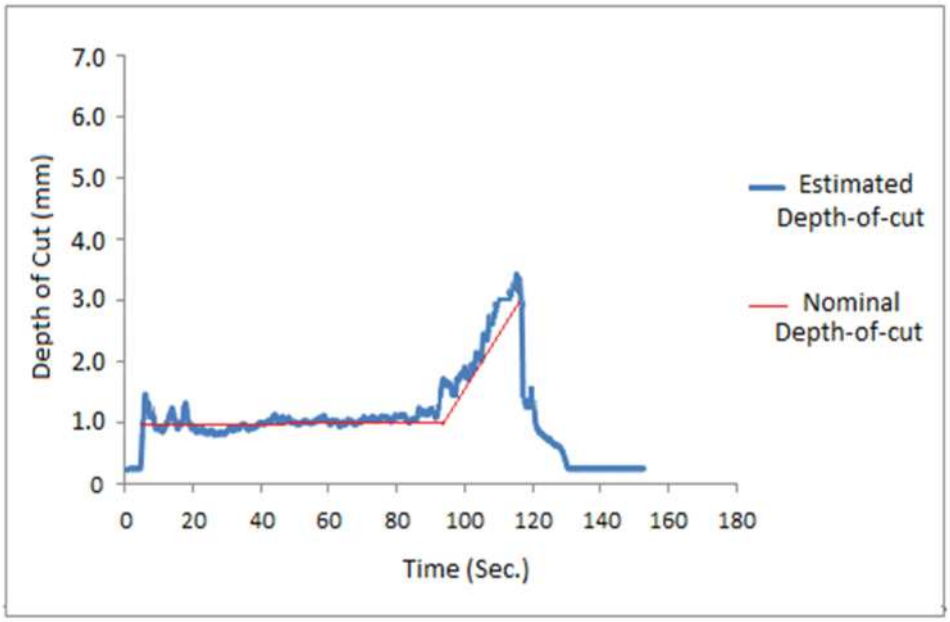
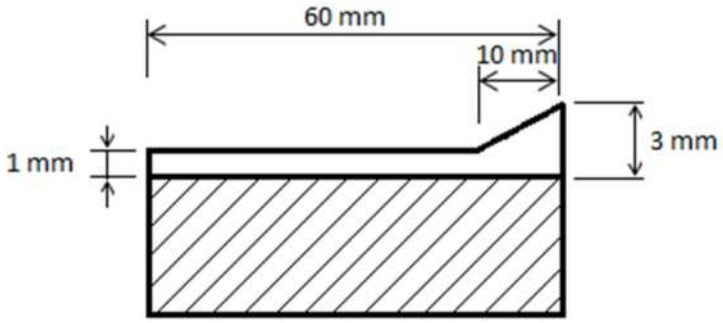


Figure 5.6 Interrupted Cutting (a) Nominal/Estimated Depth-of-cut (b) Cutting Geometry



(a)



(b)

Figure 5.7 Inclined Surface Cutting (a) Nominal/Estimated Depth-of-cut (b) Cutting Geometry

As final test for the efficiency of the depth-of-cut detecting system, a free form surface was made from stainless steel 316 using laser deposition. The deposited part was first scanned using a 3D scanner, then the part was machined and scanned again as shown in figure 5.8.

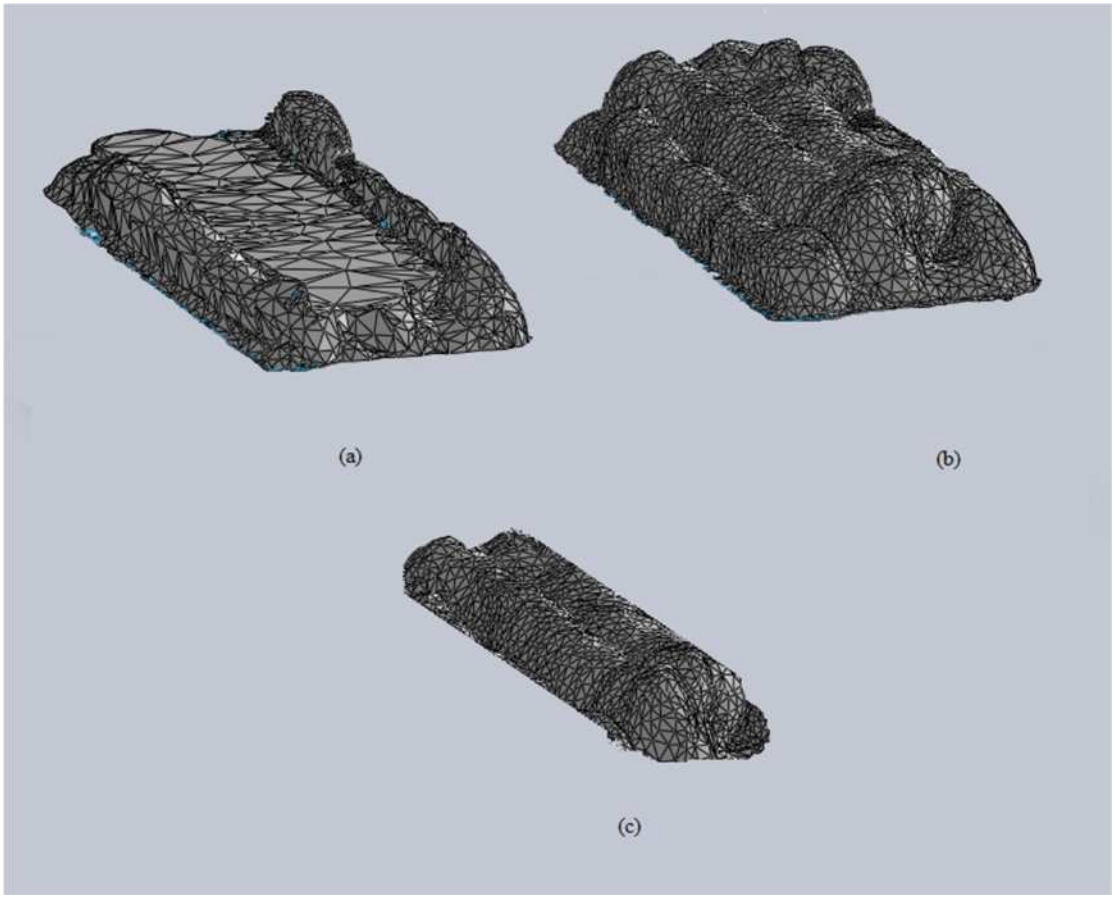


Figure 5.8 Scanned Deposited Material (a) Machined (b) Original (c) Removed

The difference between the two scans is the machined material. The machined material was sliced to fifty sections as shown in figure 5.9 and the area of each section was calculated. In order to calculate the depth-of-cut, the area of each section was divided by the tool diameter (12.7 mm) as show in table 5.1.

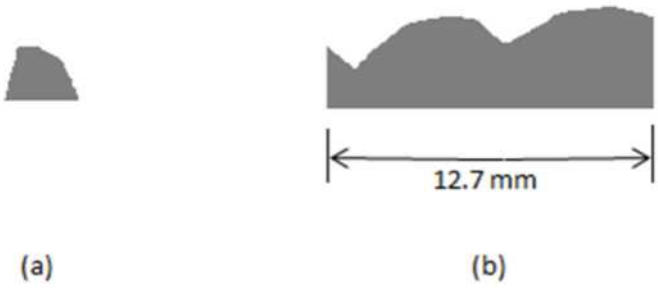


Figure 5.9 Machined Material Slicing (a) First Section. (b) Fifteenth Section.

Figure 5.10 shows the measured depth-of-cut from the sections and detected depth-of-cut by the acoustic emission sensor. The feed rate was 60 mm/min, cutting speed 4000 rpm, cutting length about 52 mm and the tool was worn-out. There is some deference between the measured and detected depth-of-cut in several points. This error might be caused by the change in the shear strength of the deposited material where the depth-of-cut detection model was made with material deposited at 800 W laser energy and the material tested now was made at 1000 W laser enegy.

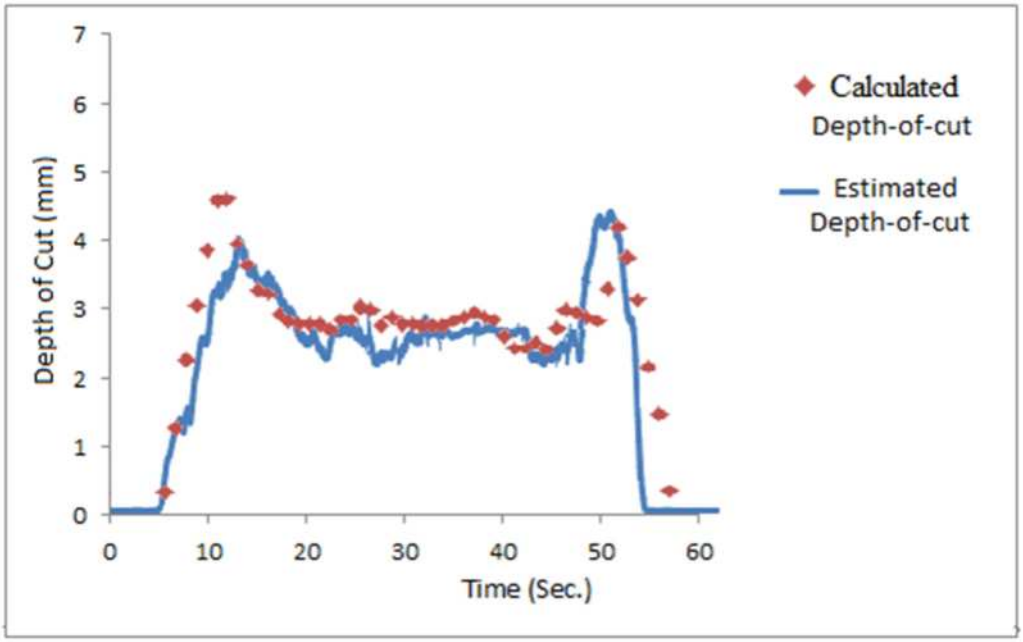


Figure 5.10 Measured and Detected Depth-of-cut for a Deposited Material

Table 5.1 The Area and Depth-of-cut of the Section

Section	Area	Depth-of-cut
1	4.239	0.333779528
2	16.257	1.28007874
3	28.94	2.278740157
4	39.072	3.076535433
5	49.302	3.882047244
6	58.481	4.60480315
7	58.81	4.630708661
8	50.586	3.983149606
9	46.573	3.667165354
10	41.807	3.291889764
11	41.096	3.235905512
12	37.481	2.951259843
13	36.036	2.837480315
14	35.521	2.796929134
15	35.394	2.786929134

Table 5.1 (Continued)

16	35.457	2.791889764
17	34.503	2.716771654
18	36.215	2.851574803
19	36.279	2.856614173
20	38.754	3.051496063
21	38.233	3.010472441
22	35.307	2.78007874
23	36.747	2.893464567
24	35.619	2.804645669
25	35.55	2.799212598
26	35.203	2.771889764
27	35.295	2.779133858
28	35.359	2.784173228
29	35.96	2.831496063
30	36.741	2.892992126
31	37.707	2.969055118
32	36.707	2.890314961
33	36.412	2.867086614
34	33.346	2.625669291
35	31.045	2.444488189
36	30.998	2.440787402
37	32.051	2.523700787
38	30.622	2.411181102
39	34.798	2.74
40	38.042	2.995433071
41	37.695	2.968110236
42	36.73	2.892125984
43	35.932	2.829291339
44	42.172	3.320629921
45	53.388	4.203779528
46	47.834	3.766456693
47	39.91	3.142519685
48	27.615	2.174409449
49	18.917	1.489527559
50	4.632	0.364724409

6. CONCLUSIONS AND RECOMMENDATIONS FOR FUTURE WORK

6.1. CONCLUSIONS

This research investigated experimentally the depth-of-cut and the acoustic emission variations during end-milling of deposited stainless steel 316 with an uncoated tungsten carbide tool under dry conditions, and it studied the correlation between the acoustic emission variation and the depth-of-cut. Design of experiments was used to conduct experiments. As a result of this work, as innovative regression model was developed to predict depth-of-cut in end milling.

The experimental values were used to develop the regression model. The experimentally determined depth-of-cut values were compared with values predicted by the model, and the model is proved to be capable of predicting depth-of-cut with the acceptable margin of error. The results indicate that this model is robust and accurate.

The proposed depth-of-cut prediction method demonstrates how depth-of-cut can be controlled by adjusting machining parameters within the constraints for specific machining conditions. This study provides a depth-of-cut monitoring system for more efficient manufacturing in the future.

6.2. FUTURE WORK

Future work will investigate signal processing and feature extraction since the root mean square is provided by the coupler and there is no control on low-pass and high-pass filters. A raw signal can be acquired from the coupler, and this signal contains more information than the root mean square signal, which was already processed inside the

coupler. Also, the model in equation 6 can also be used to estimate feed rate, cutting speed or tool wear when the other cutting parameters are given.

More experimental work is needed to improve the prediction of depth-of-cut for inclined and curved surfaces, but since the vast majority of end-milling operations result in parallel surfaces, the inaccuracy of such predictions are unlikely to limit the use of the system under normal circumstances.

In the future, more detailed experiments will permit the construction of mathematical relationships between the change depth-of-cut and the change in workpiece dimensions and tool offset. This mathematical model will be used to predict depth-of-cut and optimization of the cutting process for new combinations of tool and workpiece materials, tool geometries, and cutting conditions.

BIBLIOGRAPHY

[1] Liang S., D. Dornfeld, “Tool wear detection using time series analysis of acoustic emission,” J. Eng. Ind. Trans ASME 111(3):199–205, 2009

[2] Li X., “A brief review: acoustic emission method for tool wear monitoring during turning,” Int J Mach Tools Manuf 42:157–165, 2002.

[3] KannateyAsibu E. and D. A. Dorndeld, “Quantitative relationship for acoustic emission from orthogonal metal cutting,” Trans ASME 103:330–340, 1981.

[4] Micheletti G. F., W. Koenig and H. R. Victor, “In-process tool wear sensors for cutting operations.” Annals of the CIRP 25, pp. 483–488, 1976.

[5] ASM Handbook: Nondestructive Evaluation and Quality Control, vol. 17 (Materials Park, OH: ASM, p. 284, 1992).

[6] Goebel K., W. Yan, “Feature selection for tool wear diagnosis using soft computing techniques,” In: The ASME International Mechanical Engineering Congress and Exhibition, Orlando, pp. 5–10, 2000.

[7] Kaiser J.- Untersuchungen uber das Auftreten Geraushen beim Zugversuch (An Investigation into the Occurrence of Noises in Tensile Tests). PhD dissertation, Technische Hochschule, Munich Germany, 1950.

[8] Ravindra H., Y. Srinivasa, R. Krishnamurthy, “Acoustic emission for tool condition monitoring in metal cutting,” Wear 212 (1) 78–84, 1997.

[9] Chen X., Beizhi Li, “Acoustic emission method for tool condition monitoring based on wavelet analysis,” Int. J. Adv. Manuf. Technol. 33: 968–976, 2007.

[10] Li X., Z. Yuan, “Tool wear monitoring with wavelet packet transform- fuzzy clustering method,” Wear 219 (2) 145–154, 1998.

[11] Choi J. G., and Yang, M. Y, "In-Process Prediction of Cutting Depths in End Milling," Int. J. Mach. Tools Manuf., 39(5), pp. 705–721. [Inspec] [ISI] , 1999

[12] Yang Liuqing, DeVor Richard, Kapoor Shiv, “Analysis of Force Shape Characteristics and Detection of Depth-of-Cut Variations in End Milling,” J. Manuf. Sci. Eng. 127, 454 , DOI:10.1115/1.1947207, 2005.

[13] Wan M., W.H. Zhang, “Efficient algorithms for calculations of static form errors in peripheral milling,” Journal of Materials Processing Technology 171, 156–165, 2006.

[14] Li, H., and Shin, Y. C., "A Time-domain Dynamic Model for Chatter Prediction of Cylindrical Plunge Grinding Processes," ASME J. Manuf. Sci. Eng., (in press), 2006.

[15] Yonggang Kang, Wang Zhongqi, Wu Jianjun, and Jiang Chengyu, “Numerical prediction of static form errors in the end milling of thin-walled workpiece,” IET Conf. Pub. 816, DOI:10.1049/cp:20060872, 2006.

[16] Prickett, Paul, Siddiqui, Raees, Grosvenor, Roger , “The development of an end-milling process depth of cut monitoring system,” The International Journal of Advanced Manufacturing Technology, 10.1007/s00170-010-2711-6, 2010.

[17] Teti R., K. Jemielniak, G. O’Donnell, D. Dornfeld , “Advanced Monitoring of Machining Operations,” CIRP Annals - Manufacturing Technology 59 (2010) 717–739.

[18] http://faculty.ksu.edu.sa/hossainy/Book2/9159X_05.pdf. Manufacturing Systems, 2000 (March 3, 2011).

[19] ASM Handbook: Nondestructive Evaluation and Quality Control, vol. 17 (Materials Park, OH: ASM, 1992), p. 284.

[20] ISO 8688-2, (1989). Tool Life Testing in Milling – Part 2: End Milling. International Standard, first edition.

[21] Kannatey-Asibu E Jr, Dornfeld DA, “Quantitative relationship for acoustic emission from orthogonal metal cutting,” Trans ASME 103:330–340(1981).

[22] American Society for the Testing Materials. Standard definitions of terms relating to acoustic emission, STM E610-82, 1982.

VITA

Haythem Gaja was born on May 10, 1979 in Libya. He received his bachelor degree in Mechanical Engineering in March 2003 from Al fateh University.

In August 2009, he enrolled in the Missouri University of Science and Technology for graduate studies in Manufacturing Engineering. He has been a research assistant under Dr. Frank Liou. He received his Master of Science of Manufacturing Engineering in 2011.